Electrochemical Water Ionization for Energy Storage and Water Desalination

A thesis submitted to

Indian Institute of Science Education and Research (IISER), Pune

In partial fulfilment of the requirements for the

BS-MS Dual Degree Programme

By

Digvijay Pralhad Ghogare

Registration Number: 20151177

Supervisor

Dr. Muhammed Musthafa O.T.

Associate Professor, Department of Chemistry

Indian Institute of Science Education and Research, Pune

Dr. Homi Bhabha Road, Pashan

Pune-411008

INDIA

Certificate

This is to certify that this dissertation entitled **"Electrochemical Ionisation of Water for Energy Storage and Water Desalination"** towards the partial fulfilment of the BS-MS dual degree programme at the Indian Institute of Science Education and Research, Pune represents study/work carried out by **Digvijay Pralhad Ghogare (Reg.No. 20151177)** at **Indian Institute of Science Education and Research (IISER), Pune** under the supervision of **Dr. Muhammed Musthafa O.T. , Associate Professor, Department of Chemistry, IISER Pune** during the academic year **2019-2020.**

Digvijay Pralhad Ghogare

BS-MS Student

Reg.No -20151177

IISER Pune.

Dr. Muhammed Musthafa O.T.

Associate Professor,

Department of Chemistry,

IISER Pune.

Date: 10 / 04 / 2020

Place: Pune

Declaration

I hereby declare that the matter embodied in the report entitled **"Electrochemical Ionisation of Water for Energy Storage and Water Desalination"** are the results of the work carried out by me at the **Department of Chemistry**, **Indian Institute of Science Education and Research (IISER), Pune**, under the supervision of **Dr. Muhammed Musthafa O.T.,** and the same has not been submitted elsewhere for any other degree.

Digvijay Pralhad Ghogare
BS-MS Student
Reg.No -20151177
IISER Pune.

Dr. Muhammed Musthafa O.T.
Associate Professor,
Department of Chemistry,
IISER Pune.

Date: 10 / 04 / 2020

Place: Pune

Acknowledgements

This dissertation is a consequence of cumulative assistance from many individuals. At first, I would like to explicitly thank my supervisor ***Dr. Muhammed Musthafa O.T.,*** Associate Professor, Department of Chemistry, IISER Pune, for providing an excellent opportunity to work under his guidance. Illustrating the dissertation would have been impossible without his help; hence I would like to acknowledge him for his invaluable assistance that was provided during my study.

I am thankful to ***Dr. P. A. Joy,*** Chair, Physical and Materials Chemistry Division, NCL Pune, for his constant encouragement and insightful comments throughout the project.

I would like to especially thank ***Zahid Bhat, Soumodip Sur, Mahesh Itagi, Mruthunjayachari C.D***, who assisted and guided me throughout the project. I also extend my gratitude to *Alagar Raja, Manu Gautam, Sanchayita Mukhopadhyay, Neethu CD, Abdul Raafik* and all other lab members for their kind support.

I would like to acknowledge Dr. Gyana Ranjan Tripathy, ECS department, IISER Pune for allowing us to use instruments that were necessary to carry out specific experiments.

I want to thank IISER Pune for providing outstanding research facilities during the BS-MS program. I would also like to thank DST-INSPIRE for funding. Without their funding, this project could not have reached its destination.

I would like to sincerely thank all my friends for continuously supporting me throughout the project.

At last, I express my deepest gratitude towards my parents whose moral support that helped me to achieve this milestone.

Table of Contents

List of figures

Chapter 1. Introduction

Chapter 2. Experimental Section

Chapter 3. Results and Conclusion

Abstract

Industrial effluents and wastes most often are majorly in the form of metal salts which are often dumped into water bodies without further treatments. These effluents not only leads to eutrophication and other pollution hazards but also leads to a significant loss of resources. In this context, their removal from water bodies is of utmost importance for water remediation. Here, we present an electrochemical route for salt splitting to form respective acid-alkaline solution, consequently leading to an electrochemical strategy for water remediation via the generation of value-added products. We design this chemistry in such a way that, the overpotential is dramatically reduced by overcoming the enormous driving force required for the parasitic chemistry leading to almost 100% Faradic efficiency for salt splitting. The acid-alkali generated can act as a source of energy storage and can be used to increase the efficiency of various fuel cells and electrolyzers.

Chapter 1. Introduction

1.1 Need for sustainable energy conversion and energy storage:

The rapid increase in population and robust overall economy coalesced with accelerating urbanization and industrialization will result in a massive increase in energy requirements in the next few years. Average energy consumption around the world in 2018 increased to 2.3%, double the rate than in 2010[1-2]. The energy consumption around the globe is expected to increase by up to 50% by 2050[3]. In 2018, 84% of primary energy consumption across the world was from traditional sources such as coal, oil and natural gas. In contrast, renewables only accounted for 4.4%.[4] However, energy-related CO_2 emissions have increased by 1.5% annually due to the use of traditional sources in the last five years, has attributed the most for the greenhouse effect. To attain objectives of the Paris Agreement of Climate Change, managing the surge in average global temperatures well under 2 ^{0}C by the end of the 21st century needs deployment of sustainable and renewable energy sources which are vital in reducing the effect of the greenhouse gases[5]. The power sector is the largest source for carbon emission, and hence the transition to renewable energy sources and its storage would be pivotal in achieving long term climate goals. Developing efficient renewable energy generation and generations sources are essential as renewables are expected to make 50% electricity generation by 2035.[6]

Although renewables are the source of clean energy, production has been uncertain as it is affected very much by various natural factors. For example, solar and wind energy can only be harnessed only upon the availability of sunlight and wind, respectively. Hence, integrating the energy trapped from the renewables with energy storage systems can solve the problem of fluctuations in energy production and meet the massive swings of supply and demands in peak hours. Energy storage safeguards steady supply and enhances the reliability of storage systems[7].

Energy storage systems are broadly classified into four types for large scale operations: mechanical, electrical, chemical, and electrochemical [8]. Mechanical energy consists of flywheels, pumped-storage hydroelectricity which accounts most for global storage capacity of power discharged. Supercapacitors and

superconductive electromagnetic storage are examples of electrical energy storage. Chemical energy storage involves storing of energy in the form of redox-active chemicals or hydrogen gas. The examples of electrochemical energy storage are secondary (rechargeable) and flow batteries, along with regenerative fuel cell [9]. Various energy storage technologies are characterised by system power rating (power density) and discharge duration (energy density), as illustrated in Fig 1.1. These energy storage systems provide a great solution to large scale energy storage because of its characteristics features such as high energy density, resilience, low maintenance and scalability. One of the crucial points of these energy storage systems is its decreasing cost because of a sharp rise in installation in large capacities in the recent past, and the same trend is expected in the next 20 years.[10] Future developments would enhance the integrability of storage systems into large scale power grids.

(a) **(b)**

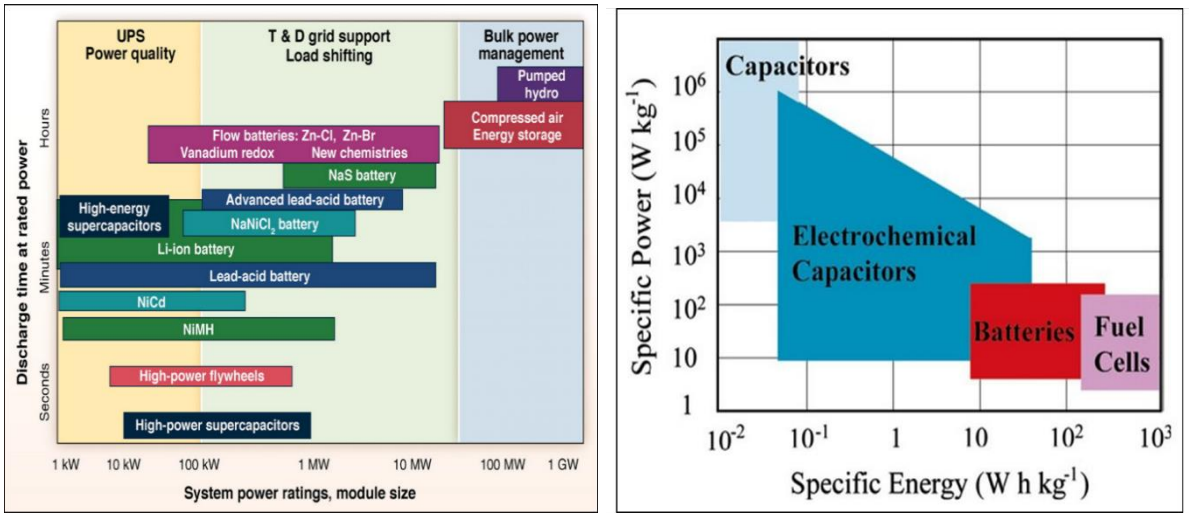

Fig. 1.1 (a) Correlation between discharge time and system power rating for various Electrochemical Energy Storage technologies. (b) Ragone plot for different energy conversion and storage system.

(a) *Electric Power Research Institute, Electricity Energy Storage Technology Options. Report 1020676, 170 (2010).*

(b) *G. Yu, X. Xie, L. Pan, Z. Bao, Y. Cui, Hybrid nanostructured materials for high-performance electrochemical capacitors. Nano Energy. 2 (2013), pp. 213–234.*

1.2 Electrochemical energy conversion and storage devices:

1.2.a Batteries:

Primary batteries are non-rechargeable cells, and they only can be discharged. The dry cell is an example of primary batteries, Fig 1.2(a). Secondary batteries are rechargeable cells which can be recharged by passing external current in the opposite direction through it and can be reused again. These electrochemical cells are based on the principle of reversible redox reactions. Batteries show high energy density, but low power density, i.e. can store a large amount of energy but cannot deliver quickly. Common examples of secondary storage are Lead-acid battery (Fig 1.2(b)), Nickel-Cadmium battery and a Lithium-ion battery (Fig 1.3).

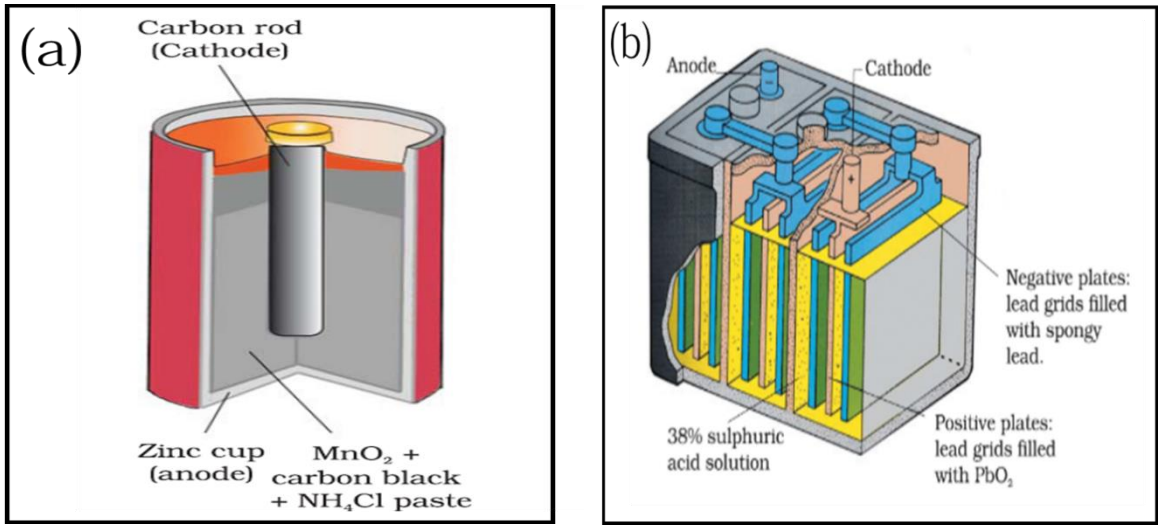

Fig. 1.2 (a) Dry cell (Leclanche cell) and (b) Lead Storage battery
Source: *(a),(b): Electrochemistry, Chemistry Part-I, Textbook for Class XII, NCERT.*

Lithium-ion batteries are based on compounds that intercalate lithium. The positive electrode is lithium metal oxide, whereas the negative electrode is graphitic carbon. Li-ions shuttles across the organic electrolyte between the electrode as Li ions can reversibly insert and remove between both the electrodes[11]. Li-ion battery is popular because of its high cell potential that corresponds to high energy density, long life cycle and excellent rate capabilities have enabled their usage in portable electronic devices and potentially in hybrid electronic vehicles in future.

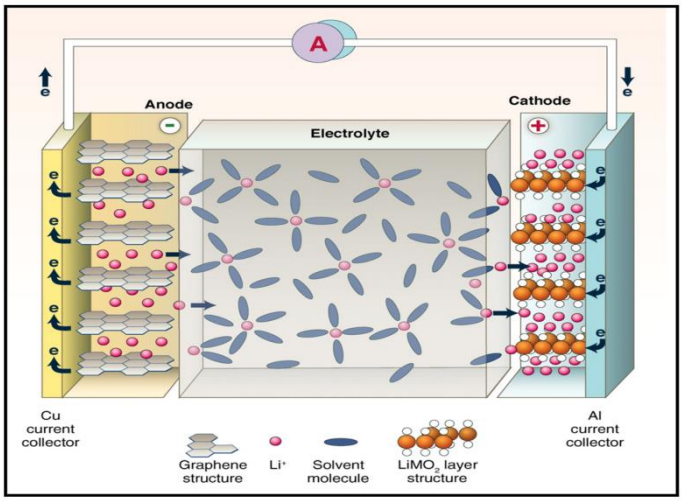

Fig. 1.3 Diagrammatic representation of a Li-ion battery

Source: *Goodenough, J.B. (2007). Report of the Basic Energy Sciences Workshop for Electrical Energy Storage.*

1.2.b Supercapacitors:

Supercapacitors are capacitors with high power density along with high energy density. This is achieved by a high surface area of the electrode and thin dielectrics which stores a higher magnitude of charge than conventional capacitors. Supercapacitors are classified on the mechanism of the charge stored: Non-Faradaic (EDLCs), Faradaic (pseudocapacitors) and Hybrid capacitors[12-13] (Figure 1.4)

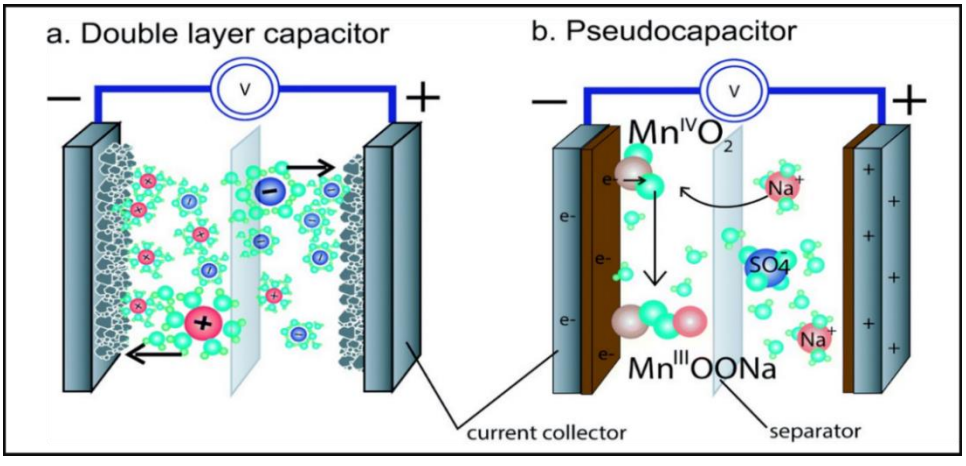

Fig. 1.4 Basic Schematics of (a) Electrochemical Double Layer Capacitor - EDLC and (b) pseudocapacitor

Source: *K. Jost, G. Dion, Y. Gogotsi, J. Mater. Chem. A, 2, 2014, 10776.*

1.2.c Redox Flow Battery:

Redox flow battery consists of electroactive redox couple species that undergo oxidation or reduction to store or deliver energy. The oxidized and reduced redox species are separated by an ion-selective membrane, which is stored in two separate tanks. Hence, the energy is stored within the electrolytes for redox flow cells, whereas batteries stores energy inside the electrode. Redox flow batteries have numerous advantages such as less damage of electrodes, less degradation of electrolytes for long time scale, flexibility and moderate cost. The battery energy capacity and power are decoupled as energy capacity depends on the size of tanks and power depends on the size of the cell (number of stacks), providing flexibility storing and delivering the energy. The typical example of a redox flow battery is Vanadium redox flow battery(Figure 1.5).[14]

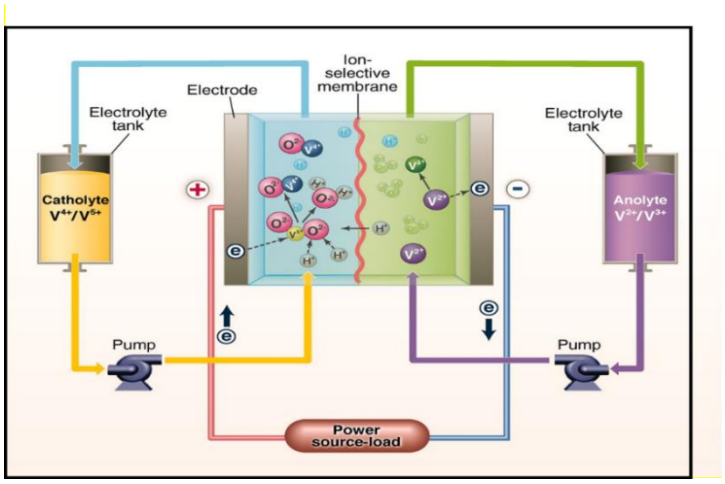

Fig. 1.5 Schematic representation of the vanadium redox flow battery as an example of redox flow batteries

Source: *Goodenough, J.B. (2007). Report of the Basic Energy Sciences Workshop for Electrical Energy Storage.*

1.2.d Fuel Cells :

Fuel Cells are galvanic cells which convert the energy of combustion of fuels such as hydrogen, methanol, methane to electrical energy. Fuel cells are different from batteries as fuel cell needs fuel to be continuously supplied to power the external load. Fuel cells consist of three segments: (1) anode, which oxidizes the fuel (2) electrolyte, which permits the flow ions between anode and cathode through it, and (3) cathode,

which reduces the oxidant such as oxygen. The classification of a fuel cell is based on the type of electrolyte being used. Common examples of fuel cells are Alkaline fuel cells (AFCs), Polymer exchange membrane fuel cell (PEMFCs), Direct methanol fuel cell (DMFCs), Phosphoric acid fuel cells (PAFCs), Molten carbonate fuel cells (MCFCs) and Solid oxide fuel cells (SOFCs)[15] (Figure 1.6). Fuel cells are considered to be a next-generation energy source because of their pollution-free operation, which can reduce the ill-impacts of fossil fuels on the environment and high energy density. Although fuel cells are efficient, the broad-scale application is hindered because of its high-cost operation associated with fuels such as hydrogen in PEMFCs and use of novel catalysts such as Platinum and Palladium.[16-19]

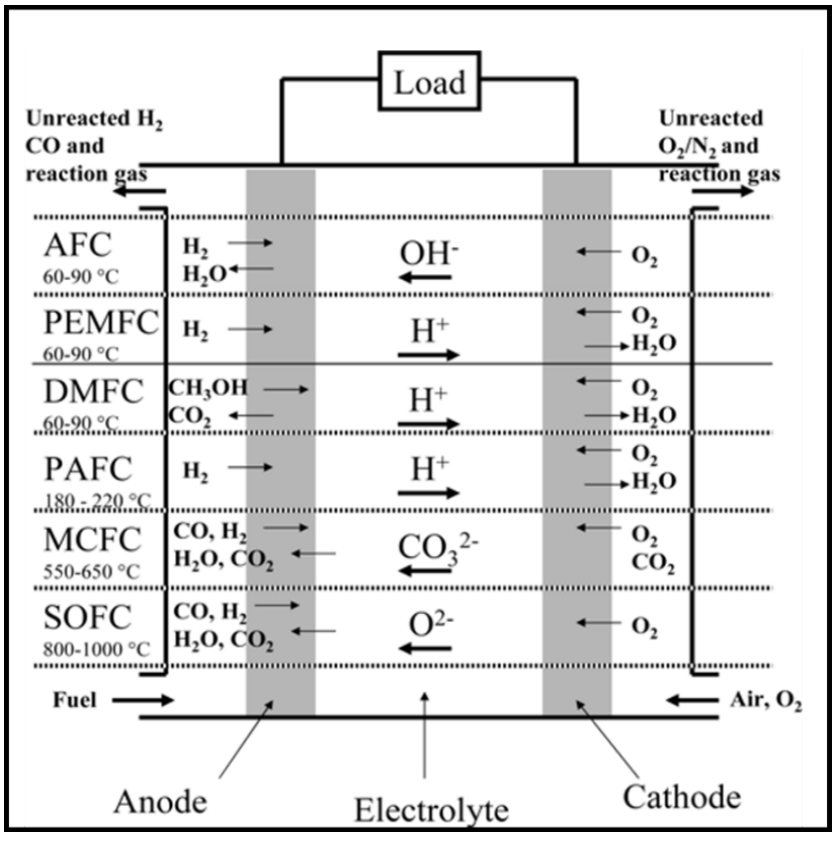

Fig. 1.6 Schematic outline of the reactions and processes that occur in different types of fuel cell systems: AFCs, PEMFCs, DMFCs, PAFCs, MCFCs and SOFCs. Source: *Chemical Reviews. 104, 4245–4269 (2004).*

1.2.e Electrolyzers :

Electrolyzers, in contrast to fuel cells, are electrolytic cells that use electrical energy to drive non-spontaneous chemical reactions to generate fuels like hydrogen, which can be stored. Water electrolyzers split water into hydrogen and oxygen using external current. Water electrolyzers are classified based upon the electrolyte (membrane) used, which depends on ions transferred between the electrodes. The ions transferred between the electrodes are H^+, ^-OH and O^{2-} and corresponding electrolyzers are called Proton exchange membrane (PEM) electrolyzer, Alkaline electrolyzer (AEL) and Solid oxide electrolyzer cells (SOEC), respectively (Figure 1.7).[20]

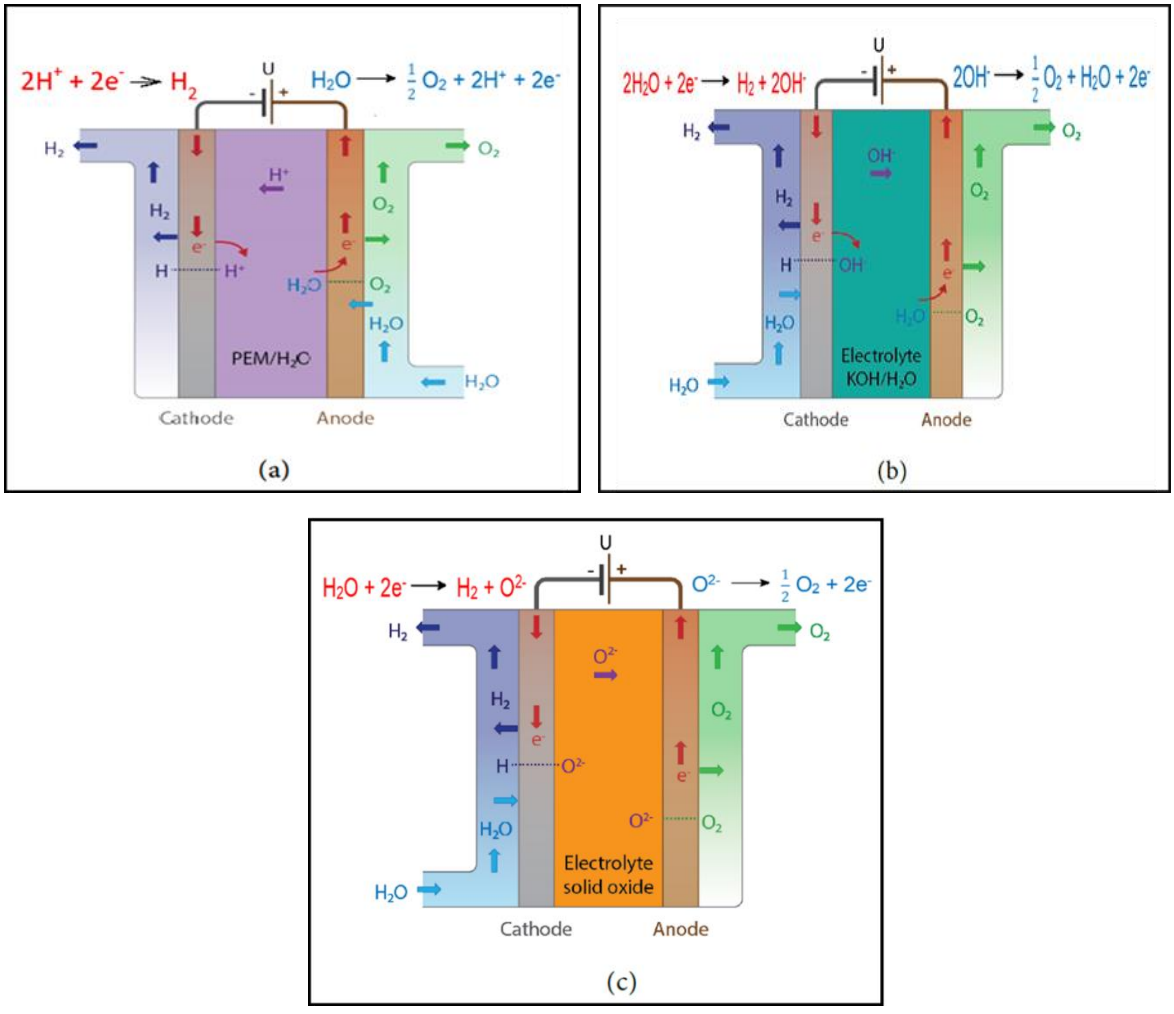

Fig. 1.7 Diagrammatic illustration of three types of water electrolyzers: (a) Proton exchange membrane (PEM) electrolyzer, (b) Alkaline electrolyzer (AEL) and (c) Solid oxide electrolyzer cells (SOEC).

N. Gallandat et al. An Analytical Model for the Electrolyser Performance Derived from Materials Parameters. Journal of Power and Energy Engineering. 05, 34–49 (2017).

1.3 Acid-Base Chemistry for energy applications:

The highly exothermic nature acid-base neutralization reaction has been realised for the conversion of chemical energy into electrical energy. A well-known example of acid-base neutralization chemistry being used for fuel-cell application is **fuel exhaling fuel cell** [21]. The energy of neutralization is converted to electrical energy gives an electromotive force of **0.828V** (Fig. 1.8 (a)). Hydrogen acts as an electron donor, producing H^+ ions neutralizing the base present in the anodic compartment whereas H^+ from the acid acts as an electron acceptor, produces H_2 gas at the cathodic compartment. The hydrogen gas produced can power another fuel cell, which can double the output energy from the same fuel. Also, hydrogen can be generated from a membrane-based on acidic/alkaline amphoteric water electrolysis Fig. 1.8 (b), which requires potential as low as **0.401 V** (theoretically) as compared to **1.23 V** (theoretically) in highly sluggish water electrolysis[22]. Hydrogen is generated under acidic condition, and oxygen evolves in an alkaline solution in acidic/alkaline amphoteric water electrolysis. Overall, acid-base acts as a catalyst for the generation of hydrogen. Hence, acid-base can be realised as a source of energy as well as a tool for energy storage.

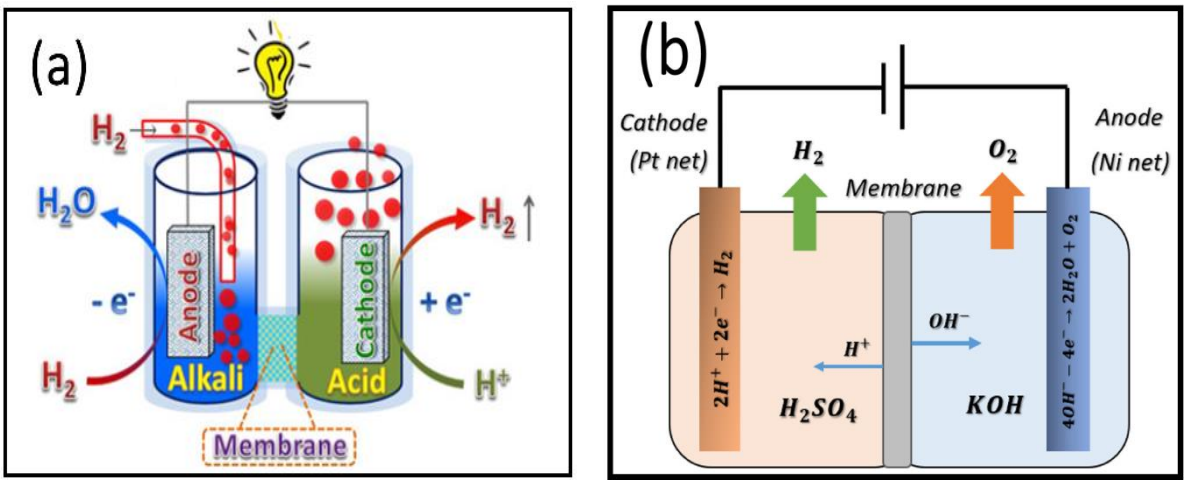

Fig. 1.8 (a) Fuel-Exhaling fuel cell and (b) acidic/alkaline amphoteric water electrolysis.

The generation of acid-base electrochemically done by water oxidation and water reduction in **water splitting reaction (WSR)**, the process requires a very high potential of **2.05 V** theoretically**.** Further, it requires high overpotentials associated with sluggish Oxygen evolution reaction (OER) at the anode [23]. This sluggish nature

hinders the energy storage using acid-base as the production of acid-base itself requires more potential (approx. 2.5 times) than energy produced from neutralization. Hence looking forward to alternative redox chemistry for energy applications using acid-base becomes critical.

1.4 Water Desalination:

Safe Drinking water and sanitation are regarded as basic fundamental human rights. Although 71% of the earth's surface is covered with water, less than 1% of total water is safe for drinking and fit for daily household application [24]. By 2025, it is predicted that water shortage would affect 48% of the total global population and 90% of available freshwater would be depleted [25]. This problem is worsened by water pollution of water bodies because of the massive discharge of effluents from industries into the water bodies.

A large number of inorganic salts such as sodium sulfate are discharged into the water bodies every year by organic synthesis processes, commodity products such as detergents, industrial activities such as kraft paper manufacturing, pharmaceuticals and agricultural drainage. The high concentration of sodium sulfate effluent is resistant to biodegradation [26]. Sulfate has been known to cause laxative effects and diarrhoea for short terms in humans [27-28]. Hence, recovery of sodium sulfate from the effluent must be made to avoid pollution of water bodies. Desalination of salt-water is done by removing the salt ions to produce freshwater. The conventional desalination technologies are membrane-based reverse osmosis (RO) and multi-stage flash distillation based on the energy input required. Membrane-based reverse osmosis needs high electrical energy input and are susceptible to membrane fouling and require periodic replacement [29-32]. Multi-stage flash distillation uses thermal energy which requires heating above 90 ^{0}C transcends to high power consumption [33-34]. Electrochemical processes such as electrodialysis (Figure 1.9(a)), ion concentration polarization and capacitive deionization (Figure 1.9(b)) hold an essential role for sustainable and economical desalination[35].

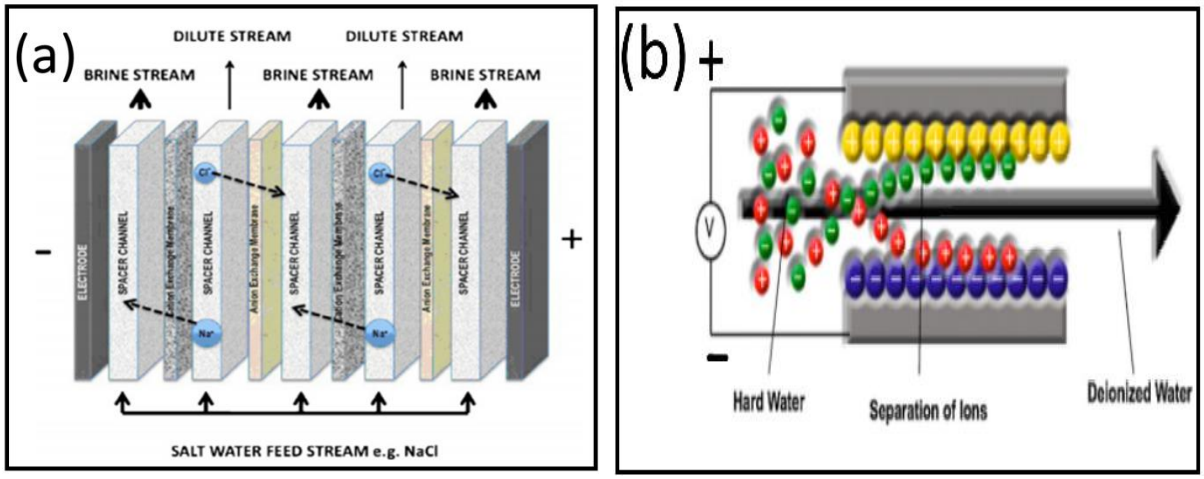

Fig. 1.9. Schematic diagram of (a)electrodialysis and (b)capacitive deionization
Source: *Electrochimica Acta.* ***55*** *(2010), pp. 3845–3856.*

Salt-splitting of sodium sulphate by water splitting reaction (WSR) is considered an effective way as it desalinates the water and produces acid-base simultaneously. However, salt-splitting of sodium sulphate is affected by the requirement of high potentials due to the sluggish nature of water splitting reaction [36-39].

1.5 Aim of dissertation:

To address the issues mentioned in **1.3** and **1.4** regarding water splitting reaction (WSR**)** pathway, we report here an electrochemical pathway for exclusive generation of acid and alkali. The highly sluggish OER of water electrolysis is replaced by facile hydrogen oxidation reaction (HOR) which is then decoupled from the hydrogen evolution reaction (HER) by an ionically conducting membrane. We name this pathway as **hydrogen oxidation and hydrogen evolution (HOHE) pathway**. HOHE pathway is investigated for its thermodynamic and kinetic parameters with respect to the **WSR pathway**. Both pathways are compared for their energy efficiencies during water remediation via the generation of value-added products by splitting the salt in aqueous solutions in a three-compartment electrolytic cell.

Chapter 2. Experimental Section

2.1 Chemicals

Sodium hydroxide (97%), sulphuric acid (98%), potassium hydrogen phosphate (98%), potassium phosphate (99%), sodium carbonate (99%), Sodium bicarbonate (99%), acetic acid (99.7%), sodium acetate (99%), potassium sulphate (99%), Iridium Oxide (99.9%), sodium sulfate (99%), Nafion® perfluorinated resin solution were bought from Sigma Aldrich India and were used as such. Pt/C was obtained from Johnson Matthey India. Nafion® 211 cation exchange membrane and Fumatec FAA-3-30 anion exchange membranes were purchased from Ion-Power, UK.

2.2 Characterization Techniques

All the electrochemical experiments such as Cyclic Voltammetry (CV), Linear Sweep Voltammetry (LSV) and Chronopotentiometry were carried out using Biologic VMP 300 electrochemical workstation. Water desalination was studied using Conductivity meter, Atomic Absorption Spectrometer (Thermo Scientific iCE 3000 Series AAS) and Ion Chromatograph (882 Compact IC plus-Metrohm). In-situ mass spectroscopy was done using Hiden HPR-40 DEMS System for gas analysis.

2.2.a. Cyclic Voltammetry (CV):

Cyclic Voltammetry (CV) is the most consistently used electroanalytical technique as it offers quantitative information on **Thermodynamic parameters** (such as formal potentials, Nernstian (reversible) or non-Nernstian (irreversible) behaviour of a redox couple, number of electrons transferred in a redox reaction) and **Kinetic parameters** (such as rate constants, diffusion coefficients) of many chemical processes.

In this technique, the three-electrode system consisting of a working electrode(WE), a counter electrode (CE) and a reference electrode (RE) is used. The potential is varied linearly forward and then reversed to the initial potential between the WE and CE using a potentiostat. The potential of WE is monitored with respect to RE. The potential of WE sweeps back and forth between two designated values because of the repetitive triangular potential excitation signal. The potentiostat records the current resulting

from the electrochemical reactions happening on the surface of the electrode. Essentially, CV measures current feedback as a function of applied potential.

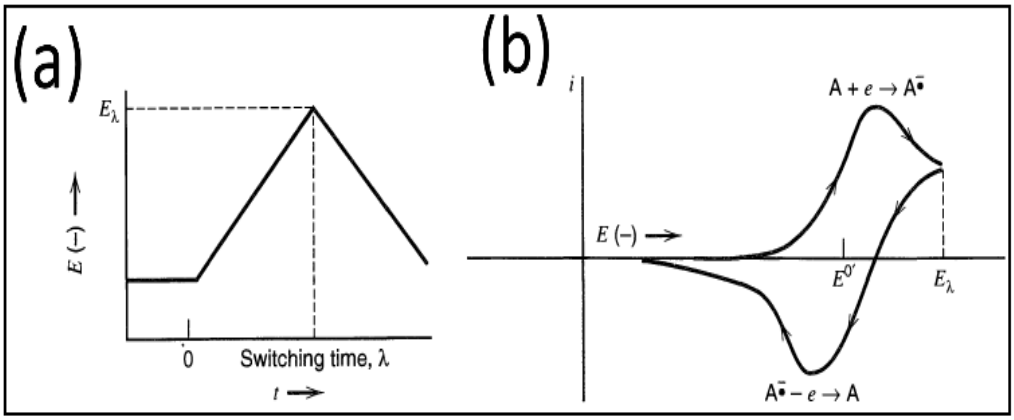

Fig 2.1 (a) Cyclic potential sweep. (b) Resulting cyclic voltammogram. Source: *Electrochemical Methods: Fundamentals and Applications, Allen J. Bard*

b. Linear Sweep Voltammetry (LSV):

In Linear Sweep Voltammetry (LSV), the potential is scanned only in the forward direction. Unlike CV, the backward scan is not performed. LSV is generally used for determining the redox potentials (onset potential) and kinetic parameters.

c. Chronopotentiometry:

The Chronopotentiometry is a galvanostatic polarization technique where the controlled current is held constant between the WE and CE, and potential is measured as a function of time. Common applications of Chronopotentiometry are:

(1) Characterization of electrode reactions mechanisms (For example, EC, CE, EE, ECE mechanisms, etc.).

(2) Constant Current Electrolysis:

- Analytical: measurement of n (number of electrons)
- Synthetic: Growth of conducting polymers on the electrode surface
- **Electrodeposition of Metals**
- Battery and Fuel Cells Studies (Charging and Discharging at constant current)

(3) Stripping Voltammetry for quantitative analysis of trace metal ions and organic molecules (like DNA)[40].

d. Atomic Absorption Spectroscopy (AAS):

The Atomic Absorption Spectroscopy (AAS) is a testing technique to quantify the concentration of metals at very low concentrations even in ppm or ppb ranges. The basic principle of AAS is based on atoms of different elements absorb the characteristic wavelength of light. In AAS, the liquid sample containing a dissolved element which is to be determined is introduced into the nitrous-oxide/acetylene flame. The high temperature of the AA flame splits down the sample into atoms, and the concentration of these atoms can be measured. These atoms in the sample absorb some of the electromagnetic radiation emitted from the lamp characteristic to the particular element (Fig 2.2 (b)). The more the number of atoms in the vapour state, the more radiation is absorbed. A calibration plot for the amount of light absorbed and samples of known concentration are established under similar conditions as the unknown. The amount the standard absorbs is correlated with the calibration plot, and this facilitates in determining the concentration in the unknown sample.

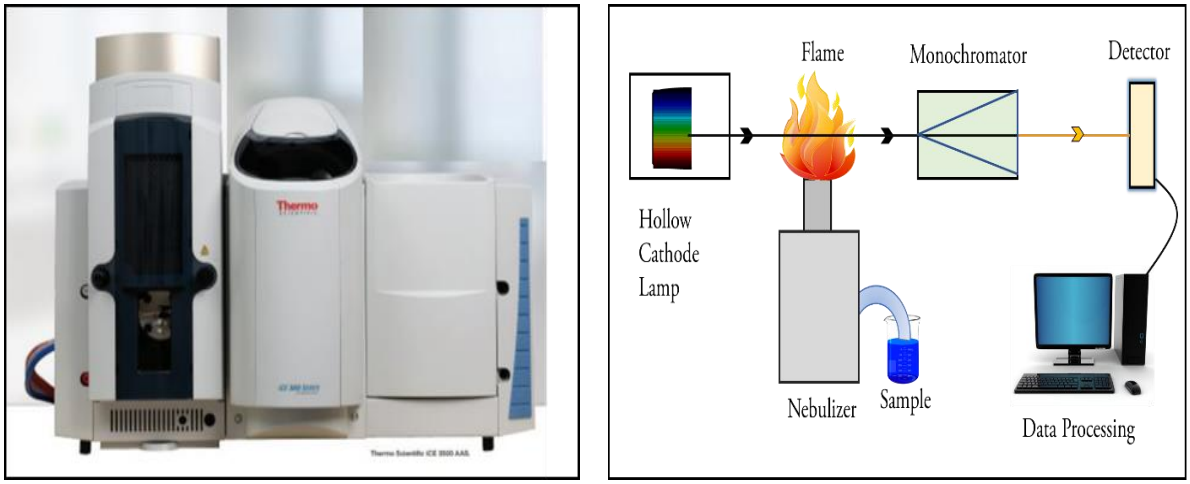

Fig 2.2 (a) Thermo Scientific Atomic Absorption Spectrometer (b) Schematics of basic working of AAS.

Source: (a) *Thermo Fischer Scientific, iCE 3000 Series AA Spectrometers Operators Manuals*

e. Ion Exchange Chromatography (Anion):

Ion exchange chromatography separates ions and polar molecules based on electrostatic interactions with the resin. In anion exchange chromatography, negatively charged molecules are loaded and are attracted towards the positively charged stationary column/resin. Ion exchange chromatography involves four steps of separation: Equilibration, Sample application and wash, Elution and Regeneration, as explained in fig 2.3. The concentration of anion is measured by UV absorbance peak profiles and conductivity traces during elution.

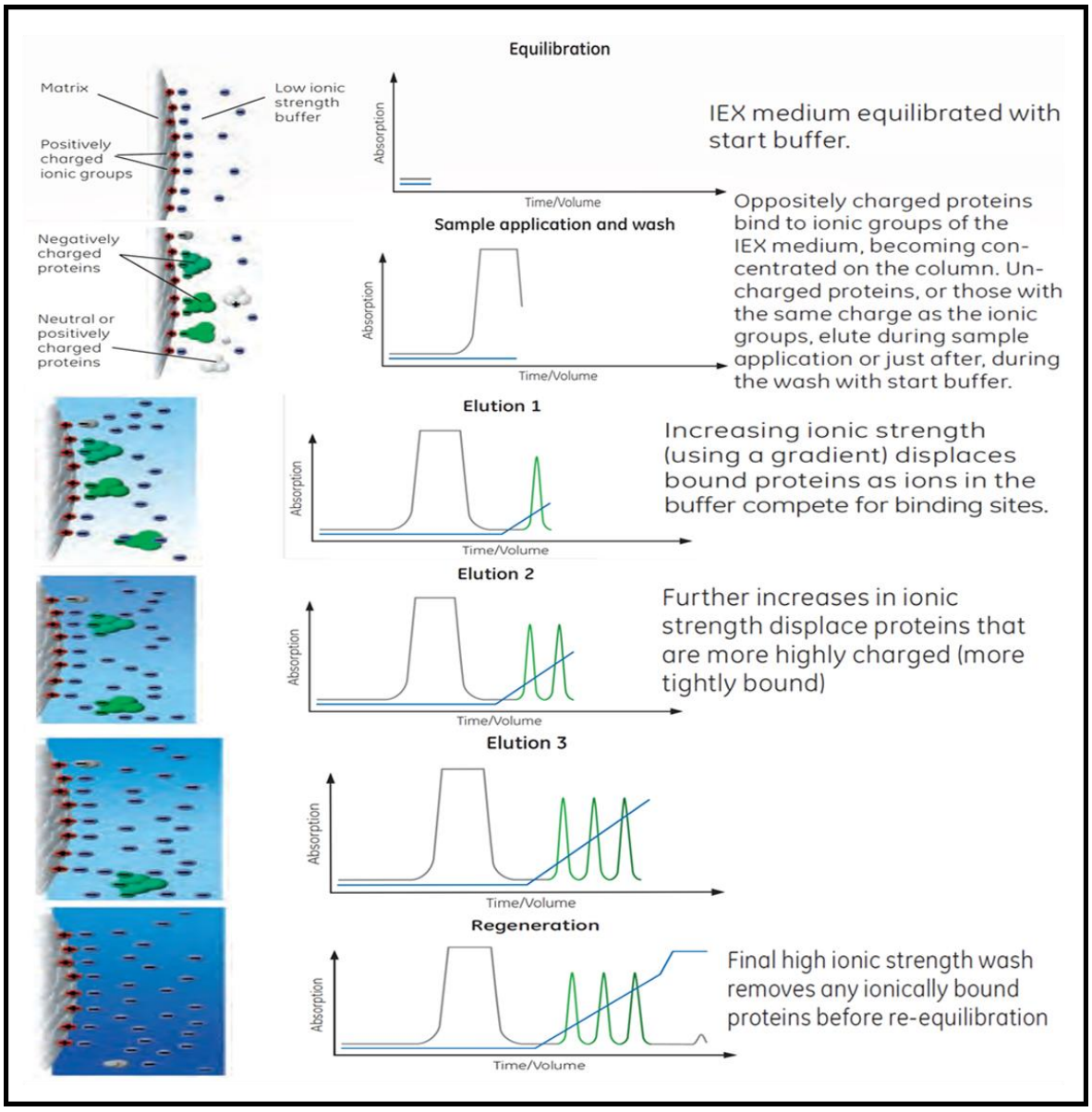

Fig 2.3 Principles of an anion exchange separation

Source: *GE Healthcare, Ion Exchange Chromatography: Principles and Methods*

f. Differential Electrochemical Mass Spectrometry:

The gaseous products evolved at the working electrodes are identified using Differential Electrochemical Mass Spectrometry (DEMS). DEM spectrometer consists of an electrochemical half-cell combined with the mass spectrometer allows detection, and time-based observation of the gaseous species evolved at the working electrode, providing insights into the in-situ reactions. The three critical components of DEMS system are half-cell, a nanoporous membrane, and a quadrupole mass spectrometer (QMS) (fig 2.4). The electrochemical half-cell performs electrochemical experimentation at a Working electrode of interest and transfers reaction products to the membrane interface. The nanoporous membrane partitions the aqueous electrolyte of the electrochemical cell from the QMS, which needs high vacuum conditions. The passage of aqueous electrolyte is avoided by hydrophobic nature of the membrane while it allows dissolved gaseous, volatile species to reach the ion source of QMS directly. These species are ionized, and formation is observed by monitoring the relevant mass ion current with QMS.

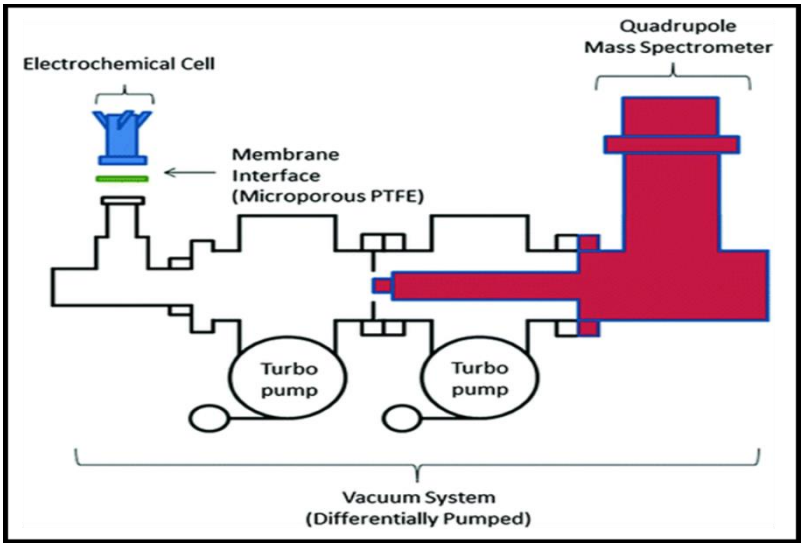

Fig 2.4 A schematic illustration of the typical components of a DEMS instrument

Ashton, S. J. (2012). Design, Construction and Research Application of a Differential Electrochemical Mass Spectrometer (DEMS).

g. Acid-Base Titration

An acid-base titration is used to determine the concentration of an unknown solution of acid-base by titrating it against a standard solution. At the endpoint, the amount of acid and base becomes equal, and the chemical reaction is called a neutralization reaction. There is a drastic change in the pH of the solution near the endpoint. If the solution becomes slightly alkaline or acidic, even a small amount of base/acid is added after endpoint, respectively. Phenolphthalein is used as an indicator in this titration. At the endpoint, phenolphthalein undergoes following changes on the addition of acid or base,

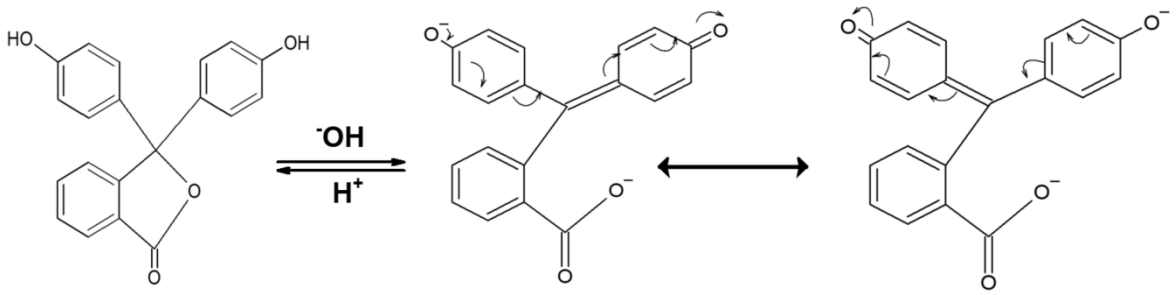

(Colourless in acid) (Pink in alkali)

The formula calculates molarity of the solution,

$$a_1 M_1 V_1 = a_2 M_2 V_2$$

where a_1, M_1, V_1 are respectively basicity, molarity and volume of acid used and a_2, M_2 and V_2 are acidity, molarity and volume respectively of base used in the titration. Oxalic acid was directly used as a primary standard for determining the strength of the base formed in the cathodic half-cell (catholyte) because of its high stability (as it is not hygroscopic and relative molecular mass is high so that weighing errors are negligible). The concentration of catholyte was determined using 0.25M oxalic acid. Sodium hydroxide was standardised using oxalic acid before determining the strength of the acid formed in the anodic half-cell (anolyte) because of the hygroscopic nature of sodium hydroxide. The secondary standard solution of 0.5M sodium hydroxide was standardised using primary standard 0.25M oxalic acid. The concentration of anolyte was determined using a standardised sodium hydroxide solution.

2.3 Procedure

2.3.a. Preparation of Buffer Solutions:

Different pH buffers solutions were made using following chemicals and monitored using pH meter : H_2SO_4 (0.5 M, pH 0), KH_2PO_4 / H_3PO_4 (pH 2), CH_3COOH / CH_3COONa (pH 4), K_2HPO_4 / KH_2PO_4 (pH 6 & 8), Na_2CO_3 / $NaHCO_3$ (pH 10), K_2HPO_4 / KOH (pH12) and NaOH (1 M, pH 14). Final pH was adjusted using 1M H_2SO_4 or 1M NaOH.

2.3.b. Preparation of IrO_2 catalyst on Titanium mesh:

10 mg IrO_2 powder was dispersed in 3 ml Isopropyl alcohol (IPA) and 10 µL Nafion® solution was added as a binder and sonicated for 45 minutes. A 2.5 x 2.5 cm^2 Ti mesh was cleaned ultrasonically in IPA for 30 minutes. IrO_2 catalyst ink was applied then on Ti mesh by brush painting. IrO_2 coated Ti mesh was then dried in the oven at 65 ^{0}C. The as-prepared electrode was used for Oxygen evolution reaction in the device.

2.3.c. Pt deposition on Stainless Steel (SS) mesh:

SS mesh (2.5 x 2.5 cm^2) was etched using 0.1M HCl for 20 seconds and then cleaned ultrasonically in distilled water and finally in acetone in a sonication bath and dried in the oven. Electrodeposition of Pt on the surface of stainless steel (SS) was carried out using Chloroplatinic acid at a constant current 1.2 mA/cm^2 for 400 seconds in conventional three-electrode setup. The SS mesh and Pt disc served as a working electrode and counter electrode, respectively. All potentials were measured against silver chloride reference (Ag / AgCl /3M KCl) electrode. The SS mesh was dried in the oven at 65 ^{0}C. The Pt deposited stainless steel electrode was used for Hydrogen evolution reaction in the device.

2.3.d. Pretreatment of Membranes:

Nafion® 211 cation exchange membrane and Fumatec FAA-3-30 anion exchange membrane, were immersed in a 0.5M Na_2SO_4 solution for 24 hours to change them

into their Na^+ and SO_4^{2-} forms, respectively and remove any additive from the membrane.[41]

2.3.e. Two-compartment cell assembly:

For **HOHE** pathway, the cell was assembled with **Pt/C based electrode** on the anodic side for hydrogen oxidation (HOR) Whereas **IrO_2 coated Ti mesh-based electrode** was used on the anodic side for oxygen evolution (OER) for **WSR** pathway. Pt deposited SS mesh was used on the cathodic side for hydrogen evolution in both WSR and HOHE pathway cells. The anodic and cathodic compartments were separated by pretreated Nafion® 211 cation exchange membrane. The membrane is placed in between the silicon gaskets to prevent electrolyte leaking across the compartments. 0.6 M Na_2SO_4 and 0.1 M Na_2SO_4 were used as electrolytes in anodic and cathodic compartments respectively. Small openings were made to pass gas in or to let evolved gas out on both sides. These compartments are entirely closed and sealed with adhesive glue to prevent in any leakage.

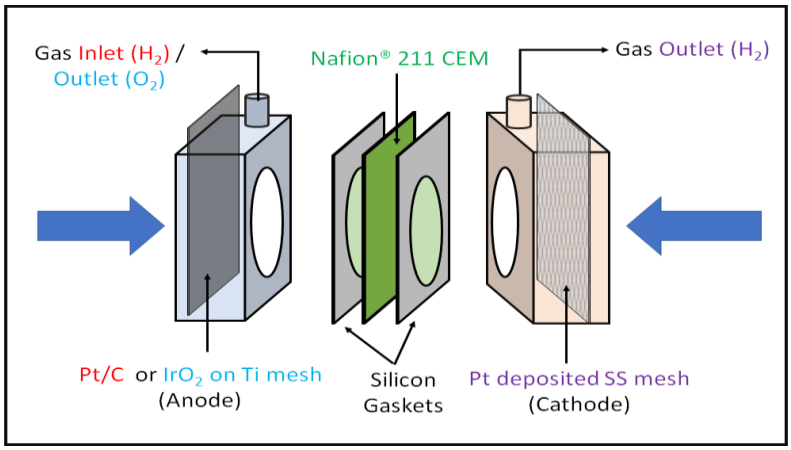

Fig 2.5 Diagrammatic representation of two-compartment cell assembly

2.3.f. Three-compartment cell assembly:

In three-compartment cell assembly, the anodic and cathodic compartments are separated by the middle compartment contains high concentrations of salt. Pre-treated Fumatec FAA-3-30 AEM is placed between anodic and middle compartment whereas Pre-treated Nafion® 211 CEM is placed between cathodic and middle compartment.

Membranes are kept in between silicon gaskets when placed between the two compartments. The electrolyte in the anodic and cathodic compartments was 0.1 M Na_2SO_4 and 1M Na_2SO_4 in the middle compartment. In **HOHE** pathway cell consists of Pt/C based electrode on the anodic side, whereas IrO_2 coated Ti mesh-based electrode is used in **WSR** pathway Cell. Pt deposited SS mesh is used on the cathodic side in both the cells.

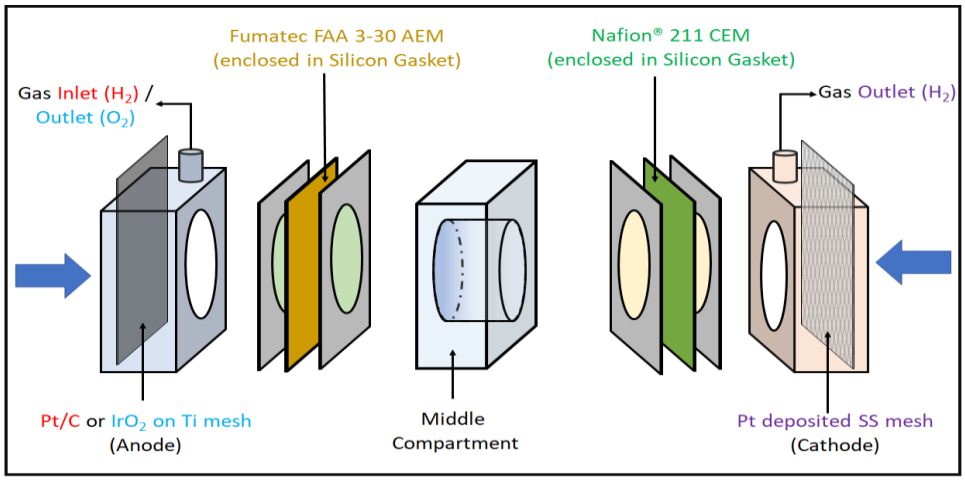

Fig 2.6 Diagrammatic representation of three-compartment cell assembly

2.4 Electrochemical Measurements

2.4.a. pH dependence of Hydrogen Evolution Reaction (HER) and Hydrogen Oxidation Reaction (HOR) using CV

pH dependence nature of Hydrogen Evolution Reaction (HER) and Hydrogen Oxidation Reaction (HOR) were studied using CV in the three-electrode configuration. For this purpose, Pt electrode (1.75 mm diameter) and Pt disc were used as Working Electrode and Counter electrode respectively. Ag/AgCl/Cl^- (3.5M KCl) was chosen as Reference electrode. Before CV, the buffer solutions were purged with N_2 gas then saturated by H_2 gas for 15 minutes. Cyclic Voltammograms were recorded in the potential range of 0.5 V to -1.2 V at a scan rate of 20 mV/s.

2.4.b. pH dependence of Oxygen Evolution Reaction (OER) using LSV:

The pH dependence nature of Oxygen Evolution Reaction (OER) was studied using LSV in three-electrode configuration. Here IrO_2 drop cast on to the Glassy Carbon (GC) electrode was used as Working Electrode. Pt disc and Ag/AgCl/Cl^- (3.5M KCl) were used as Counter Electrode and Reference electrode, respectively. LSV was recorded in the potential range of 0 V to 1.5 V at a scan rate of 5 mV/s for this study.

2.4.c. LSV and Chronopotentiometry Analysis :

The onset potential for both systems in two and three compartments was determined from LSV profiles in the two-electrode configuration. The two and three compartments cells were assembled in a configuration, as mentioned in 2.3 (e) and (f) respectively. The electrolytes in all the compartments are purged with N_2 to remove dissolved oxygen. Linear sweep scan curves were recorded in the potential range of 0 V to 4 V at a scan speed of 5 mV/s.

The constant positive current (Chronopotentiometry) is applied across the cell based on the LSV i-V profile to generate acid as well as alkali in two separate compartments. The acid and alkali are formed based on redox reactions of HOR/OER and HER, respectively. All the chronopotentiometry experiments were carried out at 40 mA for both short time interval (0.2M H^+ and ^-OH) and long time interval (1M H^+ and ^-OH).

2.5. Electrolyte and gas analysis:

Electrolyte analysis before and after the chronopotentiometry experiments were carried using pH meter for pH changes, conductivity meter for conductivity changes, and the concentration of acid and alkali formed by acid-base volumetric titration. Changes in the concentration of Na^+ ions and SO_4^{2-} ions were determined from Atomic Absorption Spectroscopy (AAS) and Ion Exchange Chromatography (IES), respectively. The real-time quantitative analysis of evolved gases was done using Hiden HPR-40 DEMS System.

Chapter 3. Results and Discussion

3.1 Abstract:

Industrial effluents and wastes most often are majorly in the form of metal salts which are often dumped into water bodies without further treatments. This not only leads to eutrophication and other pollution hazards but also leads to a significant loss of resources. In this context, their removal from water bodies is of utmost importance for water remediation. Here, we present an electrochemical route for salt splitting to form respective acid-alkaline solution, consequently leading to an electrochemical strategy for water remediation via the generation of value-added products. We design this chemistry in such a way that, the overpotential is dramatically reduced by overcoming the enormous driving force required for the parasitic chemistry leading to almost 100 % Faradic efficiency for salt splitting.

3.2 Introduction:

Even though ~71% of the earth surface is covered with water, the availability of potable water has alarmingly shrunk with an explosive rise in the global population [42]. The ultimate solution for this problem is seawater, however its high salinity of ~35 g/L makes it unfit for drinking or irrigation purposes [43]. Most of the industries produce large amounts of salts which are often discharged into water bodies without any primary treatments[44]. This leads to eutrophication and water pollution, causing various environmental issues[45]. For example, sodium sulphate forms as a significant by-product in various industrial and chemical processes, mainly when acid-base neutralization reaction involving sulphuric acid and caustic soda occurs [46]. On the other hand, preserving the sodium sulphate has little industrial significance, discharging the so formed sodium sulphate to water bodies beyond permissible limit leads to significant water pollution. These environmental complications include resistance to biodegradation [26]. Drinking of sodium sulphate contaminated water beyond the permissible limit is reported to cause laxative effect and diarrhoea in humans [47-48]. Therefore, desalination methods and the processes of salt splitting play crucial roles to provide a sustainable and rainfall independent water supply [49-50]. The state of the art processes for water desalination such as seawater reverse osmosis

(SWRO) and thermal distillation is highly energy demanding than the alternative freshwater supply from rivers and streams, groundwater, recycled wastewater etc.[51] It should be noted that other alternative methods such as capacitive deionization, electro-dialysis, shock electro-dialysis and concentration polarization involve large energy consumption per unit volume of water making them less attractive for sustainable, long-term management of growing water demand [35].

We report here an electrochemical pathway for water remediation via the generation of value-added products by splitting the salt in aqueous solutions in a three-compartment electrolytic cell. We note that simple electrolysis leads to major byproducts such as H_2 and O_2 during slat splitting leading to higher overpotential requirements for overcoming the sluggish kinetics of these reactions. This indeed affects the overall energy efficiency of the process. To overcome this parasitic chemistry and to achieve exclusive salt splitting, we have further designed new electrochemical route wherein hydrogen fuel is used to trigger the salt splitting which is then regenerated at the cathodic half-cell. This made possible almost 100% faradaic efficiency during salt splitting with a remarkably reduced overpotential.

3.3 Results and Discussion:

In conventional water splitting, the water oxidation (to produce oxygen) and reduction (to produce hydrogen) reactions are coupled as they co-occur at the anode and cathode in the same cell and requires a potential of 1.23V theoretically (equation 3.1).

$$2H_2O \longrightarrow 2H_2 + O_2 \quad | \quad E° = -1.23\ V \qquad ..(3.1)$$

However, intermediates formed in water-splitting reaction near the electrode (acid at the anode in PEM electrolyzer and base at the cathode in AEM electrolyzer) cannot be separated unless these half-cells are partitioned by a membrane to prevent the crossover of these intermediates (refer 1.2.e Electrolyzers).

Water-splitting reaction or WSR pathway can generate acid and alkali (equation 3.4) in **membrane separated anodic and cathodic half-cells** (Fig 3). The membrane decouples anodic and cathodic half-cell reaction, leading to separation of acid-base. However, this reaction, as shown in the thermodynamic calculation (calculation 1) requires a voltage of 2.05 (as discussed in 1.3).

Anode: $2H_2O \longrightarrow O_2 + 4H^+ + 4e^-$ (OER) | E° = +1.229 V ...(3.2)

Cathode: $4H_2O + 4e^- \longrightarrow 2H_2 + 4\ ^-OH$ (HER) | E° = - 0.828 V ...(3.3)

Net cell Reaction: $\mathbf{6H_2O \longrightarrow 2H_2 + O_2 + 4H^+ + 4\ OH}$ **| $E°_{cell}$ = - 2.057 V** ...(3.4)

Calculations 1:

$$\Delta_f H_{total} = \Delta_f H_{final} - \Delta_f H_{initial}$$

$$= [4\Delta_f H(H^+) + 4\Delta_f H(^-OH) + 2\Delta_f H(H_2) + \Delta_f H(O_2)] - [6\Delta_f H(H_2O)]$$

$$= [4\times (0) + 4\times (-229.99) + 2\times (0) + (0)] - [6\times (-285.83)]$$

$$= 795.02\ kJ$$

$$\Delta S_{total} = \Delta S_{final} - \Delta S_{initial}$$

$$= [4\Delta S(H^+) + 4\Delta S(^-OH) + 2\Delta S(H_2) + \Delta S(O_2)] - [6\Delta S(H_2O)]$$

$$= [4\times (0) + 4\times (-10.75) + 2\times (130.68) + (205.14)] - [6\times (69.91)]$$

$$= 4.04\ J/K$$

At standard temperatures and conditions, T = 298K and 1 atmosphere pressure

$$\Delta_f G_{total} = \Delta_f H_{total} - T\Delta S_{total}$$

$$= 795.02 - \frac{298\times(4.04)}{1000}\ kJ$$

$$= 793.816\ kJ$$

$$E_{cell} = -\frac{\Delta_f G_{total}}{nF}$$ (n = number of electrons, F – Faraday constant)

$$= -\frac{793.816\times 1000}{4\times 96500}$$

$$= \mathbf{-2.0565\ V}$$

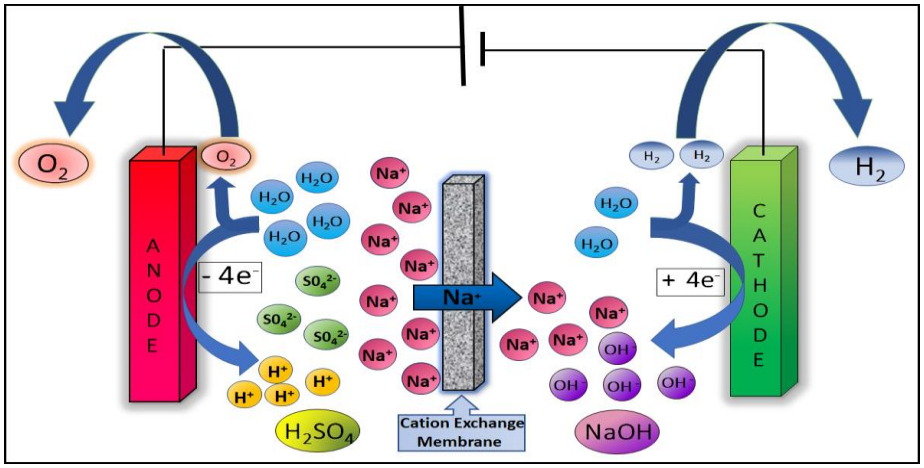

Fig. 3.1 Schematic illustration of water splitting reaction (WSR) in a two-compartment cell separated by a cation exchange membrane (Nafion® 211).

Experimentally it is indeed turned out that salt splitting occurs at **2.48 V** (Figure 3.2(a)) which is substantially higher due to the higher overpotential requirement of mainly the oxygen evolution reaction (OER). H_2 and O_2 evolutions in the ratio 2:1 are confirmed by in-situ electrochemical mass spectrometry, Figure 3.2(b) and the faradaic efficiency of water splitting process is close to 100%, Figure 3.2(c). Therefore, this process is highly energy inefficient, and the reaction pathway **does not lead to the exclusive** generation of acid and alkali as there are significant byproducts in the form of H_2 and O_2. These byproducts are, in fact, responsible for the energy inefficiency of the process.

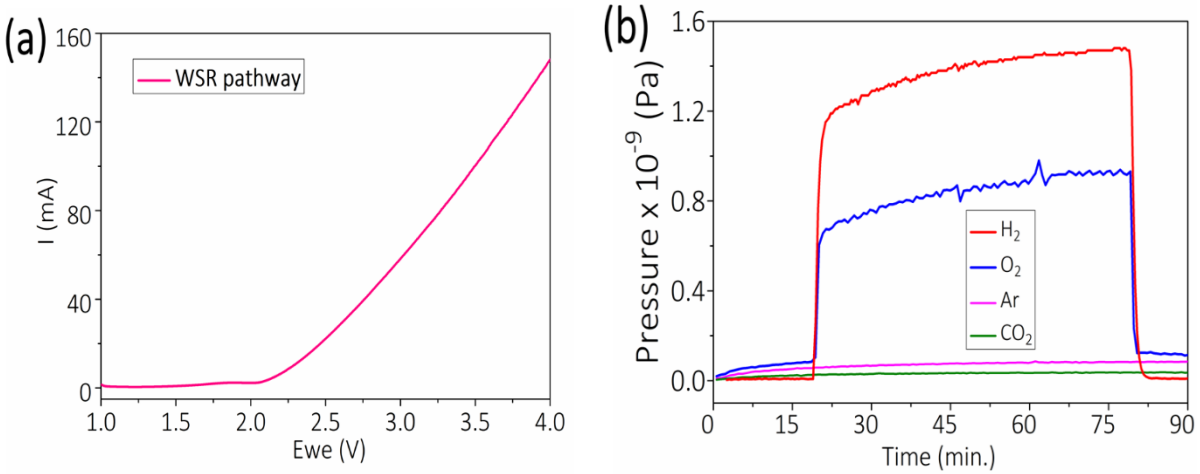

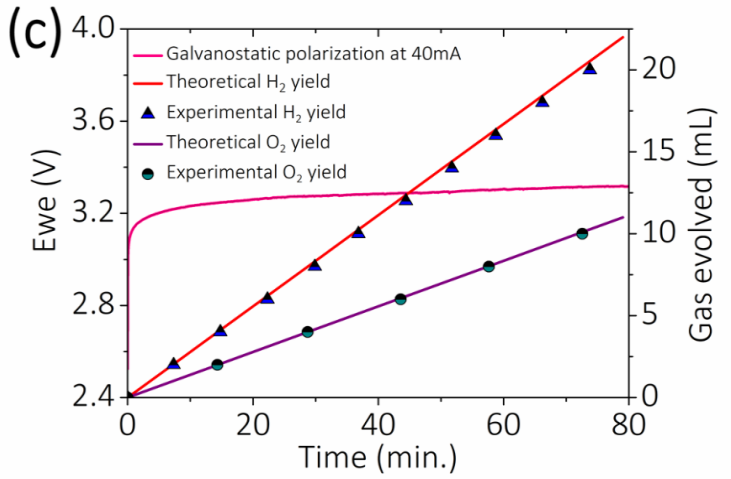

Fig. 3.2 (a) Linear sweep voltammetry (LSV) curves for WSR pathway at a scan rate of 5 mV s^{-1} (b) In-situ electrochemical mass spectrometry data for WSR pathway for gas analysis, and (c) galvanostatic polarization curve at a current of 40 mA with O_2 and H_2 quantification at the anode and cathode, respectively.

To overcome this challenge, we have designed a new electrochemical route for the **exclusive** generation of acid and alkali (equation 3.7). The schematics of this new electrochemical route is shown in Figure 3.3, and it involves hydrogen oxidation at the anodic half-cell and hydrogen evolution at the cathodic half-cell (HOHE pathway), equations 3.5 and 3.6, respectively. The thermodynamic calculation shows that the voltage requirement for this pathway is 0.826 V (Calculation 2).

Anode: $H_2 \longrightarrow 2H^+ + 2e^-$ (HOR) | $E° = +0.000$ V ...(3.5)

Cathode: $2H_2O + 2e^- \longrightarrow H_2 + 2\,^-OH$ (HER) | $E° = -0.828$ V ..(3.6)

Net cell Reaction: $2H_2O \longrightarrow 2H^+ + 2\,^-OH \;|\; E°_{cell} = -0.828$ V ...(3.7)

Calculations (2):

$$\Delta_f H_{total} = \Delta_f H_{final} - \Delta_f H_{initial}$$

$$= [2\Delta_f H(H^+) + 2\Delta_f H(^-OH)] - [2\Delta_f H(H_2O)]$$

$$= [2\times(0) + 2\times(-229.99)] - [2\times(-285.83)]$$

$$= 111.68 \text{ kJ}$$

$$\Delta S_{total} = \Delta S_{final} - \Delta S_{initial}$$

$$= [2\Delta S(H^+) + 2\Delta S(^-OH)] - [2\Delta S(H_2O)]$$

$$= [2\times(0) + 2\times(-10.75)] - [2\times(69.91)]$$

$$= -161.32 \text{ J/K}$$

At standard temperatures and conditions, T = 298K and 1 atmosphere pressure

$$\Delta_f G_{total} = \Delta_f H_{total} - T\Delta S_{total}$$

$$= 111.68 - \frac{298\times(-161.32)}{1000} \text{ kJ}$$

$$= 159.75 \text{ kJ}$$

$$E_{cell} = -\frac{\Delta_f G_{total}}{nF}$$

$$= -\frac{159.75\times1000}{2\times96500}$$

$$= \mathbf{-0.828\ V.}$$

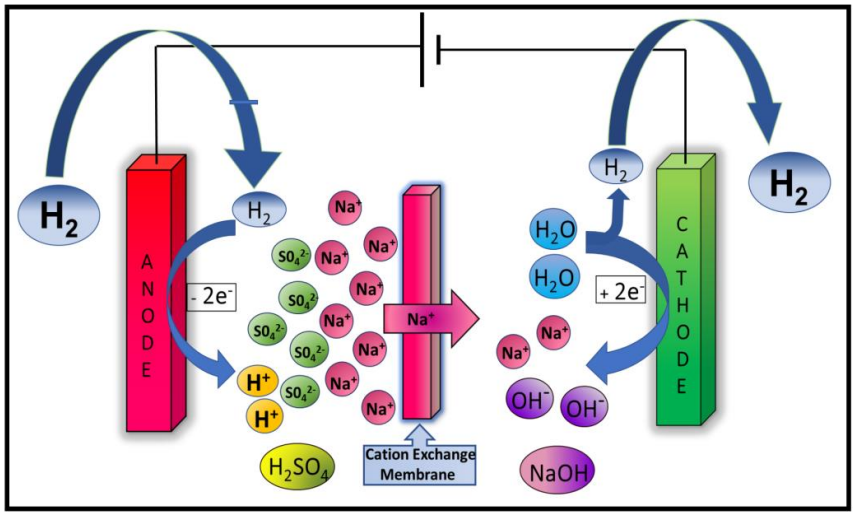

Fig. 3.3 Schematic illustration of involves hydrogen oxidation at the anodic half-cell and hydrogen evolution at the cathodic half-cell (HOHE pathway) in a two-compartment cell separated by a cation exchange membrane (Nafion® 211).

Experimentally, acid-alkali generation by this pathway occurs at remarkably lower driving force than water-splitting reaction, Figure 3.4(a). This is mainly because the new reaction pathway does not involve kinetically complex reaction such as oxygen evolution reaction as in water-splitting reaction. Hydrogen consumption in the anodic half-cell and hydrogen evolution in the cathodic half-cell in the new electrochemical route is confirmed by in-situ electrochemical mass spectrometry, Figure 3.4(b). In essence, the new electrochemical route involves the exclusive generation of acid and alkali without any byproducts at a remarkably lower electrical driving force.

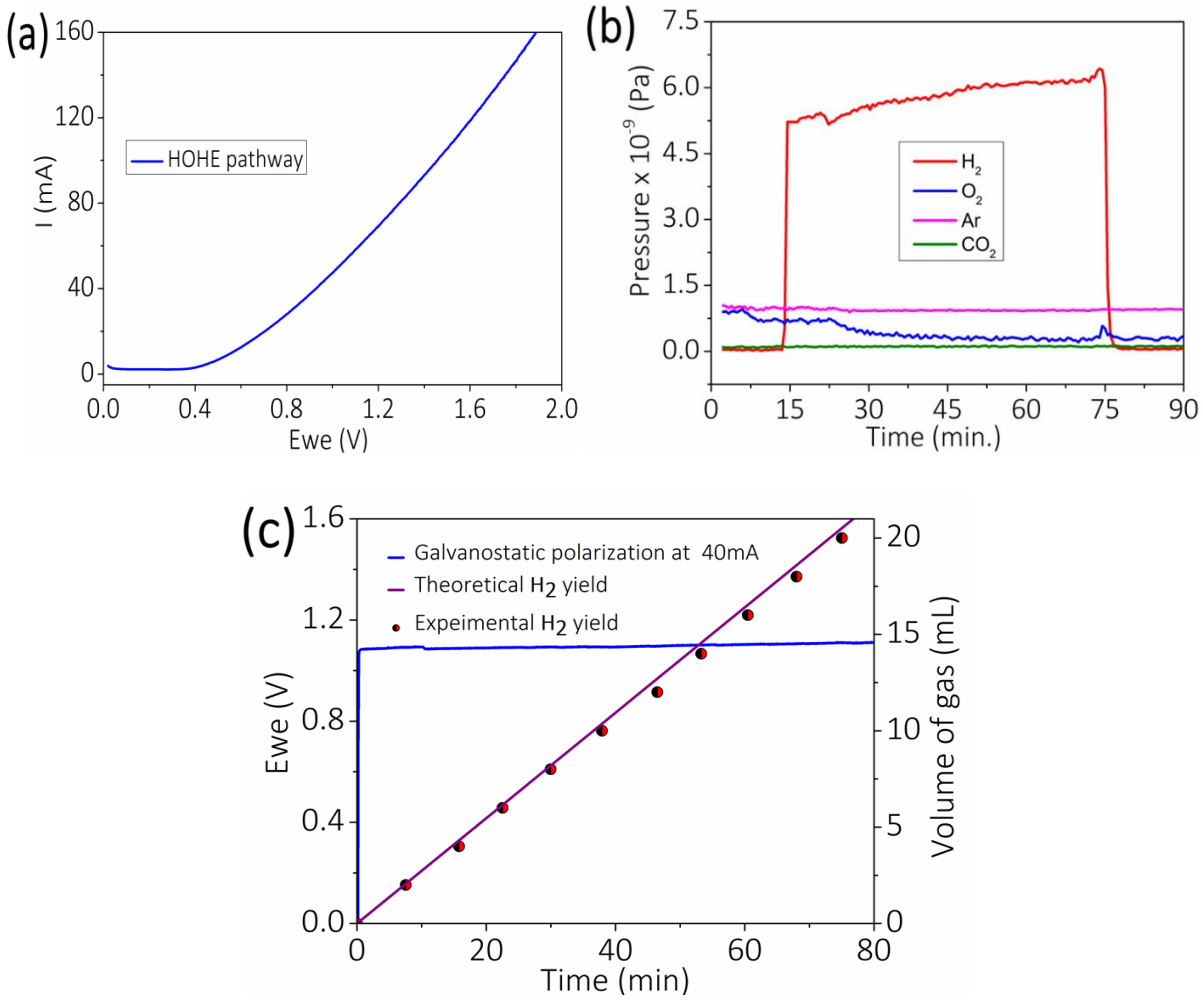

Fig. 3.4 (a) LSV curves for HOHE pathway at a scan rate of 5 mV s^{-1} (b) In-situ electrochemical mass spectrometry data for HOHE pathway for gas analysis and (c) galvanostatic polarization curve at a current of 40 mA with H_2 quantification at the cathode.

The device works on the principle of the proton dependence of the hydrogen redox reaction (hydrogen oxidation reaction (HOR) and hydrogen evolution reaction (HER)), Figure 2. These reactions shift negatively with respect to the pH, linear sweep voltammograms (LSVs) (Figure 3.5(a), 3.5(c)) and the Pourbaix diagrams (Figure 3.5(b), 3.5(d)) demonstrate a slope of **57.36 mV/pH for HOR** and **59.31 mV/pH for HER,** which is close to 59 mV/pH expected when equal numbers of electrons and protons and hydroxyl ions are transferred in a reaction. Pourbaix diagram (Figure 3(b), 3(d)) suggests that hydrogen redox reaction in pH =14 alkaline solution has a relative negative potential of -0.8 V vs. SHE compared to pH = 0 acidic solution (0 V vs. SHE), Figure 2(g). Therefore, an acidic half-cell where HOR is performed (equation 3.4) is decoupled from an alkaline half-cell where HER is performed (equation 3.5) by an ion-selective membrane, acid-alkali generation should occur at driving force as low as 0.826 V. On the contrary, OER shifts to more positive potentials in acidic media and HER shifts to more negative potentials in alkaline media, Figure 2(h), leading to a very high electrical driving force for the WSR pathway. It is also evident from equations (3.2-3.7) that amount of H^+ ions formed would be equal to the amount of ^-OH ions formed in both HOHE and WSR pathway.

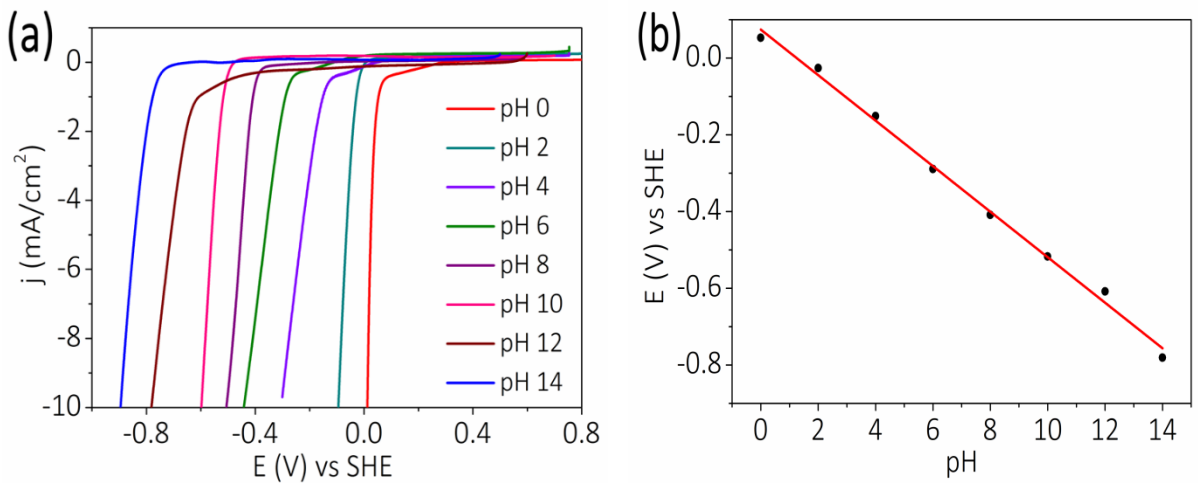

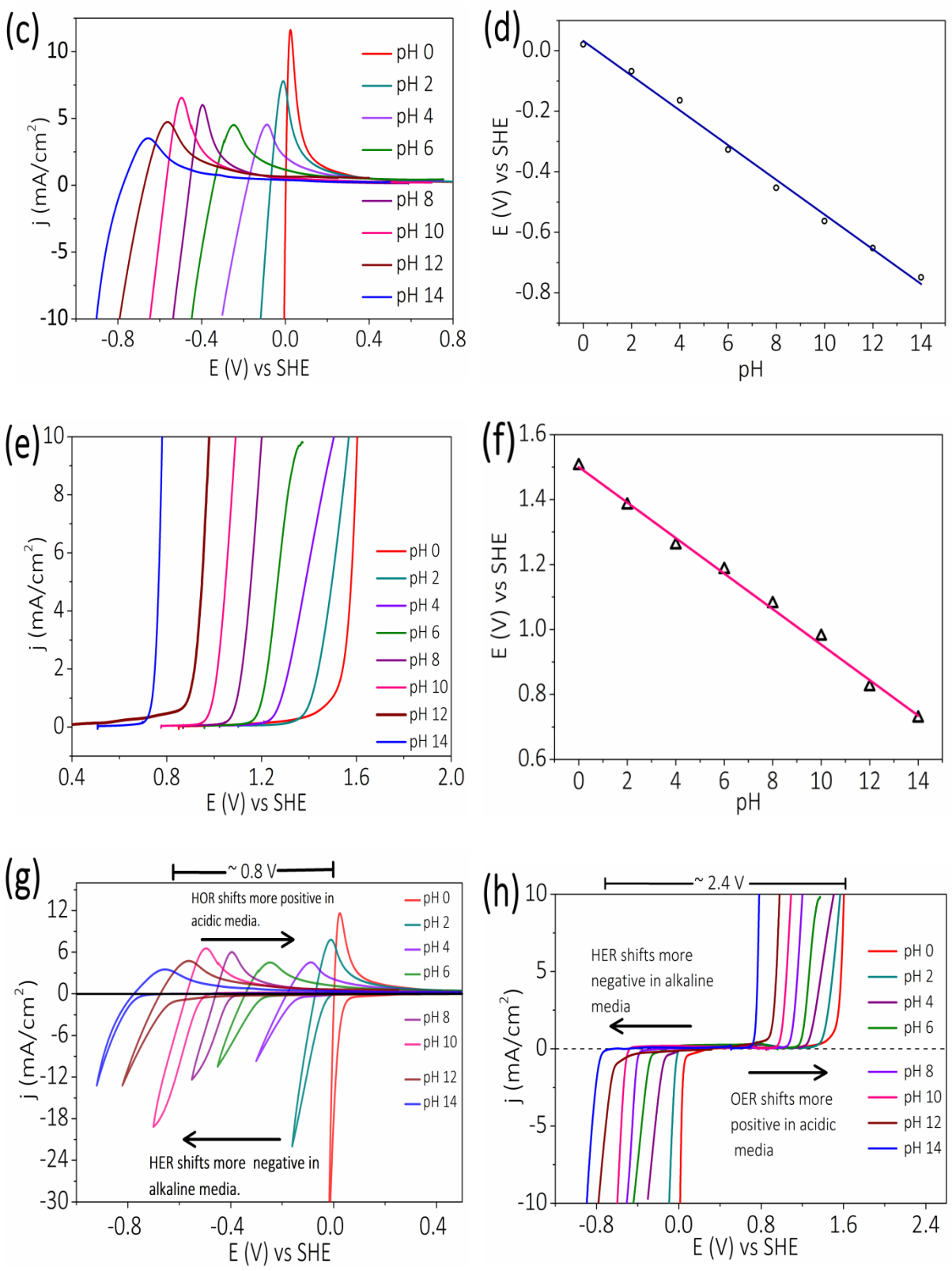

Fig. 3.5 (a) HER on the platinum electrode in different pH solutions, (b) Pourbaix diagram for HER, (c) HOR on the platinum electrode in different pH solutions (d) Pourbaix diagram for HOR, (e) OER on IrO_2 drop cast on glassy carbon electrode in different pH solutions, (f) Pourbaix diagram for HER, (g) Widening of potential

window w.r.t pH in HOHE pathway and (h) Widening of potential window w.r.t pH in WSR pathway.

The HOHE pathway is remarkably stable, and for achieving the same current density, the device required only remarkably lower overpotential than WSR pathway, Figure 3.6(a) and (b). The amount of acid and alkali generated were followed by acid-base titration and pH measurements and all these revealed acid-alkali formations close to the amount of current passed in either process, Figure 3.6(c) and (d), however at 65% reduction in driving force in HOHE process compared to WSR process (40 mA current passed for 2 Hrs.15min would generate 0.2M H^+ and ^-OH ions in 16 mL electrolyte present in each anode and cathode, respectively). The formation of acid and alkali is further proved by conductivity measurements where an increase in conductivity after the process signals the formation of acids and alkalis, Figure 3.6(e) and (f).

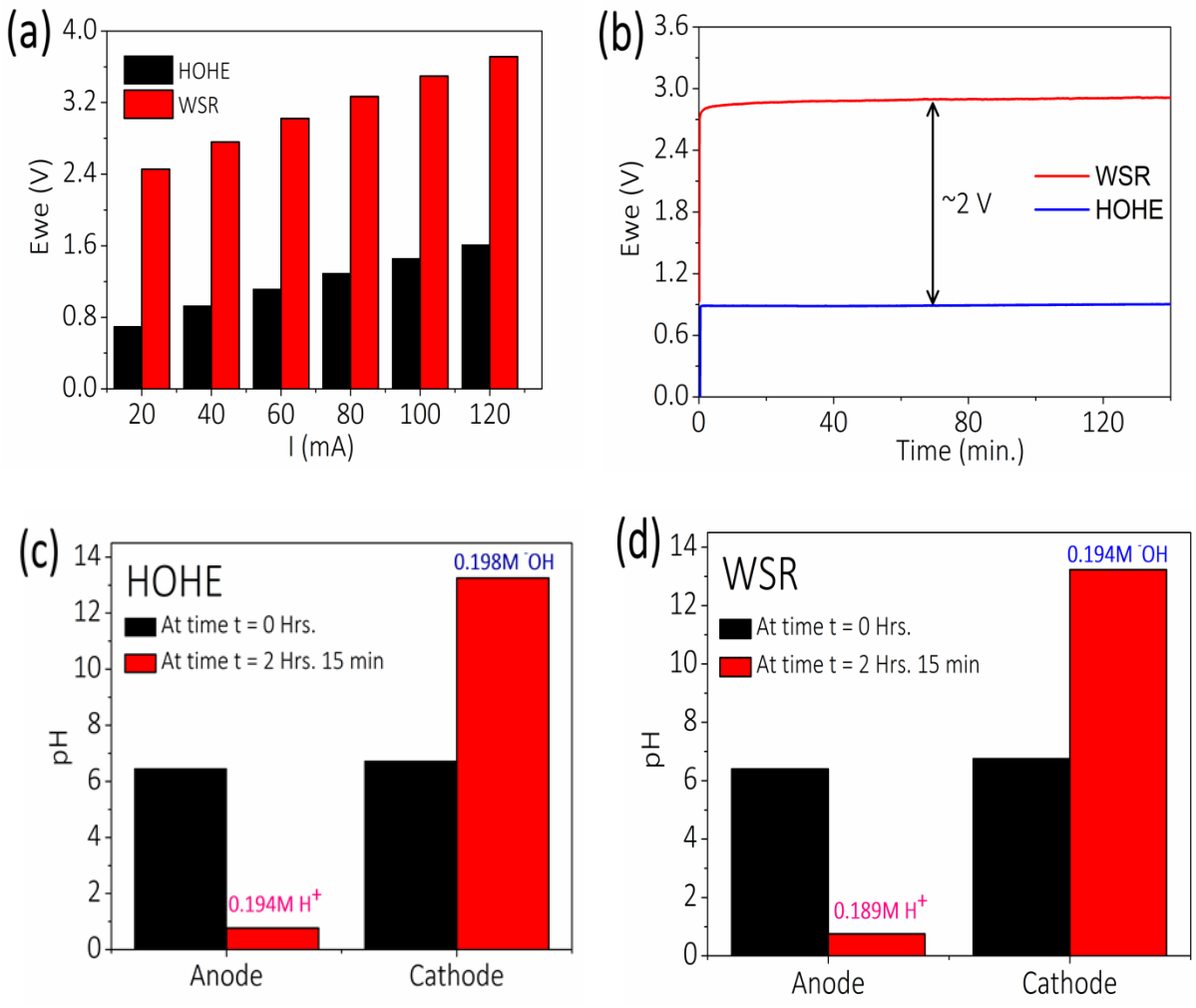

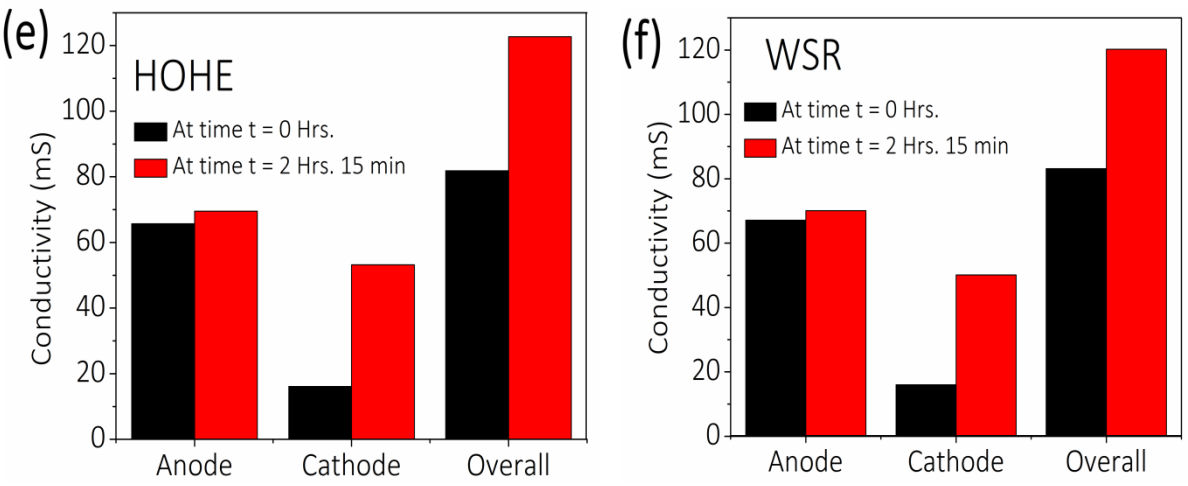

Fig. 3.6(a) Comparison of the voltages to achieve current of 20, 40, 60, 80, 100 and 120 mA in HOHE and WSR pathway, (b) galvanostatic polarization curve at a current of 40 mA in HOHE and WSR pathway to achieve 0.2M of acid and alkali. (c) pH Changes in HOHE pathway, (d) pH Changes in WSR pathway, (e) conductivity changes in HOHE pathway and (f) conductivity changes in WSR pathway.

Since HOHE pathway is more energy-efficient than WSR pathway, the former was chosen for salt splitting reaction, Scheme 3 and it consists of an anodic and a cathodic half-cell containing salt (Na_2SO_4) at lower concentration (0.1 M) and a middle compartment with salt at higher concentration (1 M). The middle compartment and the anodic half-cell is separated by an anion exchange membrane (AEM), and middle compartment and the cathodic half-cell is separated by a cation exchange membrane (CEM). This suggests that when HOHE pathway is conducted by applying salt splitting is expected in the middle compartment with the concomitant generation of acid and alkali in the anodic and cathodic half-cell respectively (equations 3.2-3.7). This is because the hydrogen consumption (oxidation) in the anodic half-cell requires the movement of sulphate ions from the middle compartment for the charge balance (equation 5). Similarly, the generation of H_2 in the cathodic half-cell necessitates the movement of cations from the middle compartment to the cathodic half-cell (equation 6). Overall, this should lead to salt splitting in the middle compartment with concomitant generation of acid and alkali in the anodic and cathodic half-cells respectively. Electrochemical performance of salt splitting using HOHE pathway is

shown in Figure 3a and 3b. As shown, WSR pathway in the same configuration for salt splitting requires tremendous electrical driving force because of the involvement of kinetically sluggish OER and this mode of salt splitting generates major byproducts such as H_2 and O_2 which are undesirable, Figure 3a and 3b.

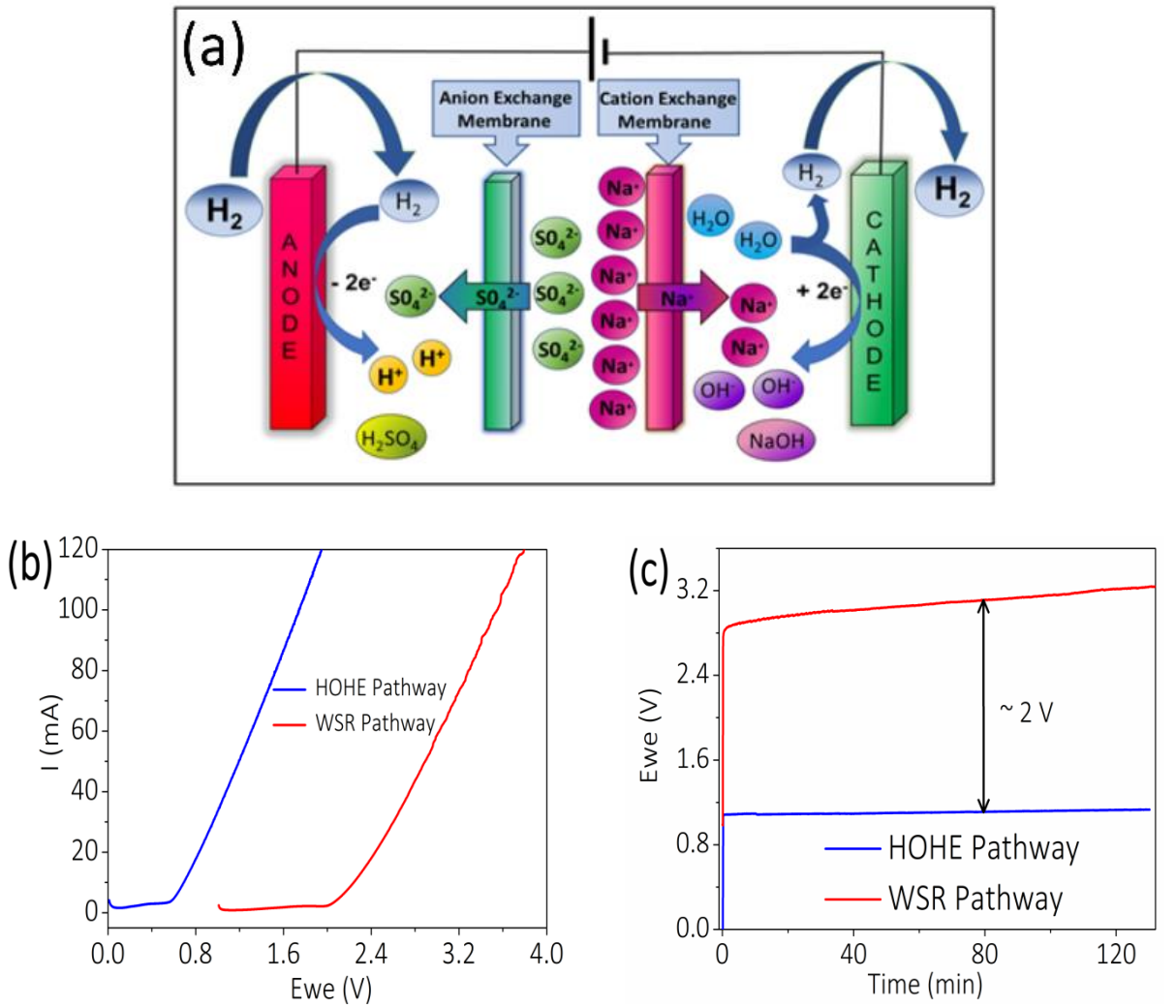

Fig. 3.6 (a) Schematic illustration of salt splitting in HOHE pathway, (b) LSV curves for HOHE pathway compared with WSR pathway for salt splitting at a scan rate of 5 mV s^{-1} and (c) galvanostatic polarization curves at a current of 40 mA in HOHE and WSR pathway for salt splitting to achieve 0.2M of acid and alkali.

The process of salt removal by HOHE pathway is monitored by atomic absorption spectrophotometry (AAS) for cation, Ion-exchange Chromatography (IEC) for anion, acid-base titration, pH and conductivity measurements. The pH measurements show

that in the anodic and cathodic half-cells, the pH changes are commensurate to the current passed with negligible pH changes in the middle compartment, Figure 3.7(a). The conductivity measurements suggest a decrease in conductivity in the middle compartment with a concomitant increase in conductivity in the anodic and cathodic half-cells, Figure 3.7(b). The number of sodium ions removed from the middle compartment is in proportion to the current passed, (Table 1) within approximately 2 hours of measurement time (Figure 3.7(c)). The same observations are made for the removal of sulphate ions, suggesting that both processes are complementary and are occurring with minimal parasitic chemistry, Figure 3.7(d). The increase in concentrations of sulfate in the anode and sodium ions in the cathode are commensurate to the current passed (Table 1) again suggesting minimal parasitic chemistry, Figure 4b. All these suggest that HOHE pathway leads to exclusive salt splitting; however, the WSR pathway leads acid-alkali formation along with the generation of H_2 and O_2 at remarkably higher voltages than HOHE pathway, Figure 5.

Table 1	Anodic Compartment	Middle Compartment	Cathodic Compartment
Initial	0.1 M Na_2SO_4 0.1 M (9600 ppm) SO_4^{2-} 0.2 M (4600 ppm) Na^+	1 M Na_2SO_4 2M (96000 ppm) SO_4^{2-} 1M (46000 ppm) Na^+	0.1 M Na_2SO_4 0.1 M (9600 ppm) SO_4^{2-} 0.2 M (4600 ppm) Na^+
Galvanostatic Polarisation @ 40 mA for 2 Hrs 15 min (for 0.2M H^+ and 0.2M OH^-)			
Final	0.2M H^+ 0.1M SO_4^{2-} (9600 ppm) 0.1 M (9600 ppm) SO_4^{2-} 0.2 M (4600 ppm) Na^+ Total SO_4^{2-} = 19200 ppm	1.8 M Na^+ (41400 ppm) 0.9 M SO_4^{2-} (86400 ppm)	0.2 M OH^- 0.2 M Na^+ (4600 ppm) 0.1 M (9600 ppm) SO_4^{2-} 0.2 M (4600 ppm) Na^+ Total Na^+ = 9200 ppm
Difference	SO_4^{2-} = 9600 ppm	Na^+ = 4600 ppm SO_4^{2-} = 9600 ppm	Na^+ = 4600 ppm

Table 1: Theoretical amount of salt splitting for galvanostatic polarization at a current of 40mA for 2 Hrs.15min.

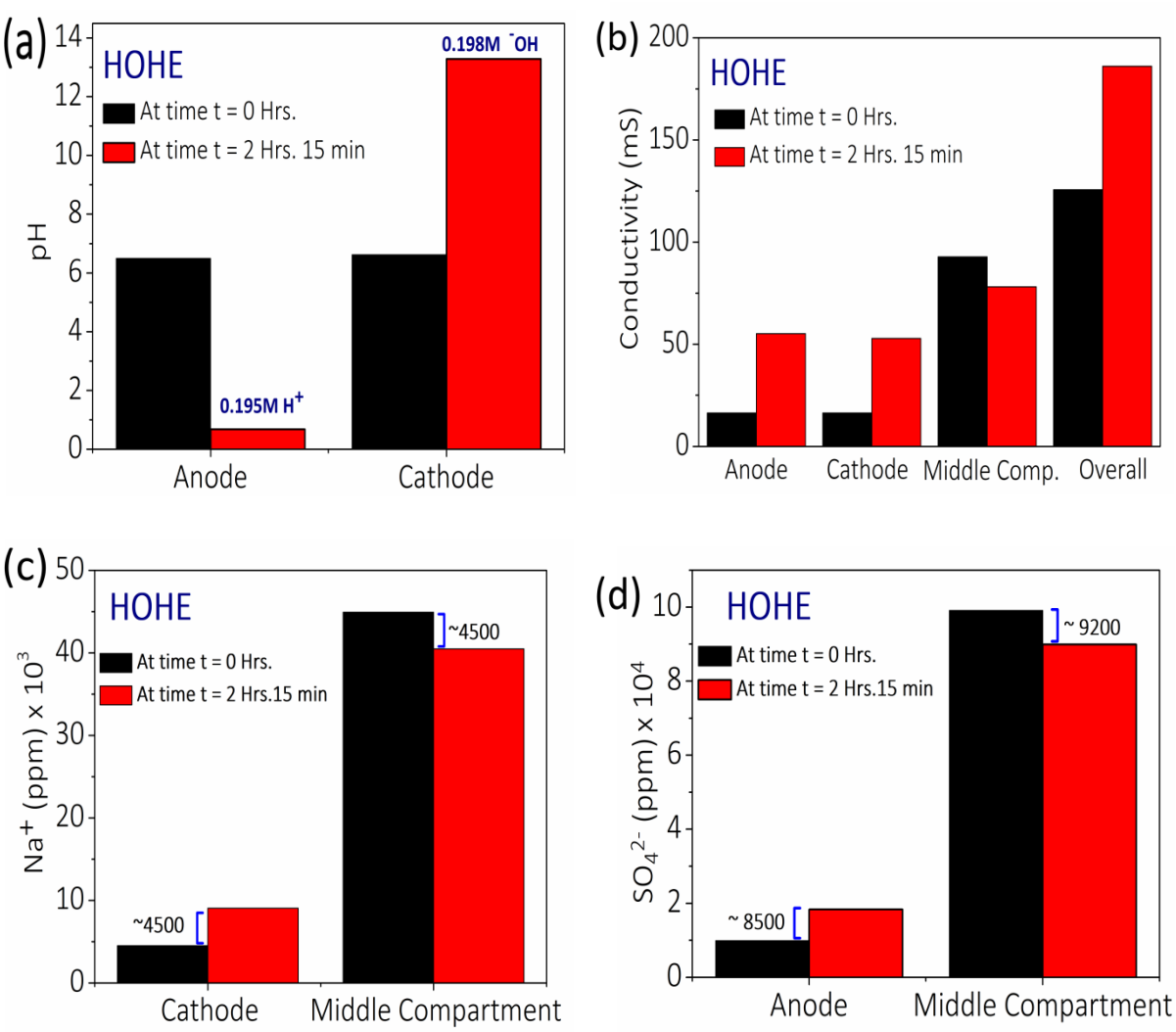

Fig. 3.7 (a) pH Changes and (b) conductivity changes, observed at anode and cathode, (c) change in Na^+ ion concentration in the cathode and middle compartment (monitored using AAS) and (d) change in SO_4^{2-} ion concentration in the anode and middle compartment (monitored using IEC). All these changes were observed for HOHE pathway at a constant current of 40 mA.

In a longer time scale, however, we have observed deviations (Figure 3.8) between the current passed (Table 2) with respect to acid-base formation and salt splitting. The yield of acid-alkali formed is very less due to the crossover of these ions across the membrane at a longer time scale. This effects on the amount of salt splitting as the experimental values are not concomitant with theoretical values. This is due to the instability of the AEM and CEM at higher acid-alkali concentrations, and we note that engineering membrane properties can address this by various strategies available in the literature.

Table 2	Anodic Compartment	Middle Compartment	Cathodic Compartment
Initial	0.1 M Na_2SO_4 0.1 M (9600 ppm) SO_4^{2-} 0.2 M (4600 ppm) Na^+	1 M Na_2SO_4 2M (96000 ppm) SO_4^{2-} 1M (46000 ppm) Na^+	0.1 M Na_2SO_4 0.1 M (9600 ppm) SO_4^{2-} 0.2 M (4600 ppm) Na^+
Galvanostatic Polarisation @ 40 mA for 10 Hrs 50 min (for 1M H^+ and 1M OH^-)			
Final	1M H^+ 0.5M SO_4^{2-} (48000 ppm) 0.1 M (9600 ppm) SO_4^{2-} 0.2 M (4600 ppm) Na^+ Total SO_4^{2-} = 57600 ppm	1 M Na^+ (23000 ppm) 0.5 M SO_4^{2-} (48000 ppm)	1 M OH^- 1 M Na^+ (23000 ppm) 0.1 M (9600 ppm) SO_4^{2-} 0.2 M (4600 ppm) Na^+ Total Na^+ = 27600 ppm
Difference	SO_4^{2-} = 48000 ppm	Na^+ = 23000 ppm SO_4^{2-} = 48000 ppm	Na^+ = 23000 ppm

Table 2: Theoretical amount of salt splitting for long term galvanostatic polarization at a current of 40mA for 10 Hrs 50 min.

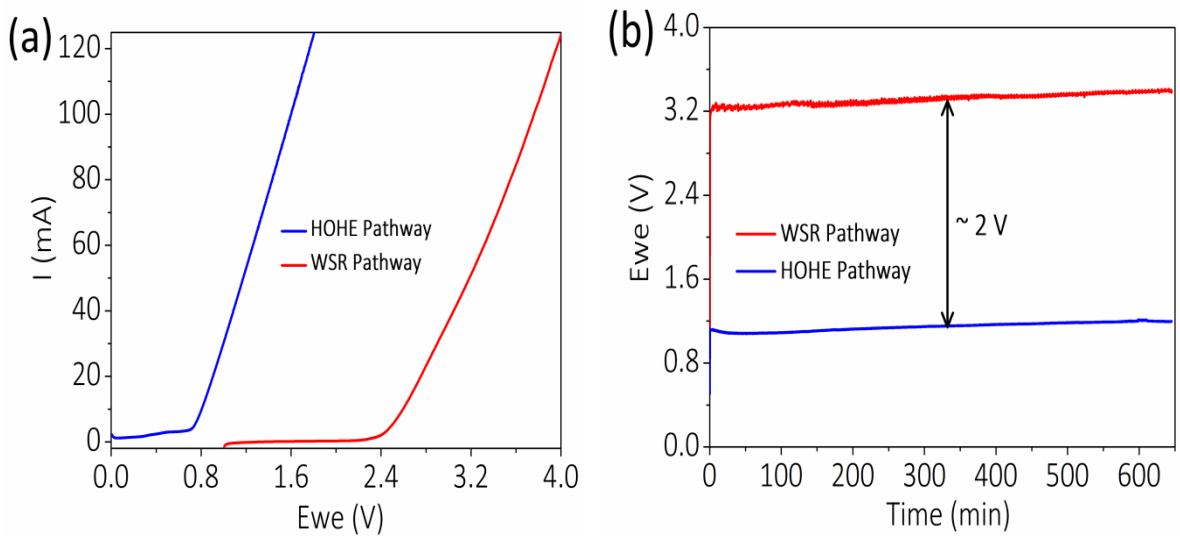

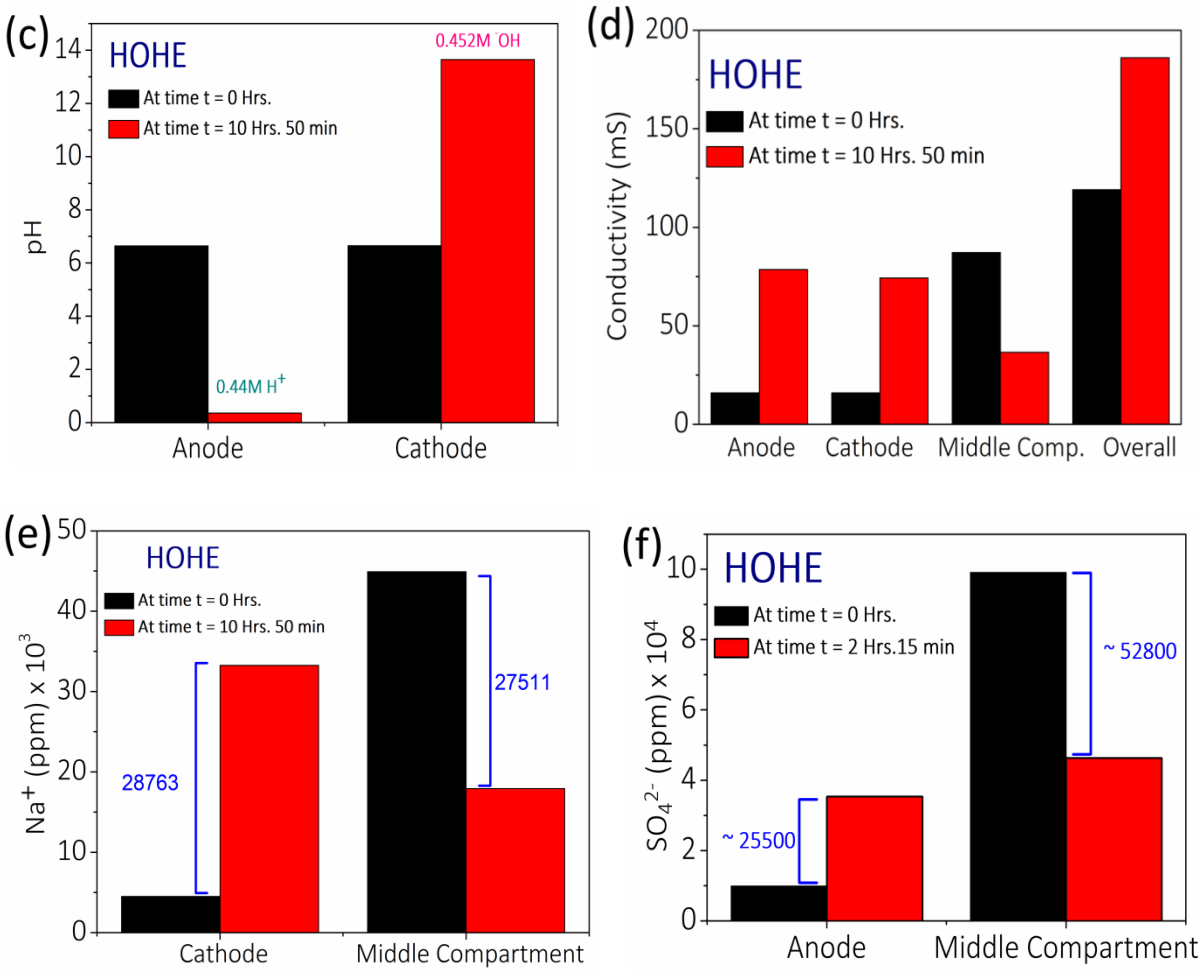

Fig. 3.8 (a) LSV curves for HOHE pathway compared with WSR pathway for salt splitting at a scan rate of 5 mV s^{-1} (b) long term galvanostatic polarization curve at a current of 40 mA in HOHE and WSR pathway for salt splitting to achieve 1M of acid and alkali (theoretically), (c) Changes in pH before and after galvanostatic polarization (d) Changes in conductivity before and after galvanostatic polarization, (e) Changes in Na^+ ion concentration in the cathode and middle compartment and (f) Changes in SO_4^{2-} ion concentration in the anode and middle compartment.

Chapter 4. Conclusions and Future Outlook

In summary, we have designed an electrochemical HOHE pathway which can store the energy of neutralization by generating acid-alkali and via electrochemical salt splitting at remarkably low potentials. This was achieved by substituting highly sluggish WSR pathway (~+2.48 V) with HOHE pathway (~+0.87 V) in which driving voltage requirement is dramatically decreased by about 66%, which is a significant step towards improving energy efficiency. For short term galvanostatic polarisation, the amount of acid-alkali generated is commensurate to the extent of charge passed, implying 100% faradaic efficiency in salt splitting in HOHE pathway. The problems associated with long term galvanostatic polarisation for retaining high concentration of acid-alkali can be solved by using modified AEM and CEM to respectively block high protons and hydroxyl ions. This would radically improve the Faradaic efficiency of the overall process of acid-alkali formation via HOHE salt splitting. The process of salt splitting by HOHE pathway could replace traditional salt splitting by WSR pathway- because of the high energy efficiency of HOHE process. Further, the HOHE process can also be an alternative to the chlor-alkali industry as the demand for Cl_2 is declining and the former can generate acid-alkali simultaneously at very low driving potentials (~0.87 V) than the latter process (which is as high as ~2.2 V). Hence, the process of HOHE pathway has high prospects in the industrial synthesis and water desalination/remediation.

References

(1) IEA (2019), "Global Energy & CO_2 Status Report 2019", IEA, Paris https://www.iea.org/reports/global-energy-co2-status-report-2019

(2) BP Statistical Review of World Energy (2019) - 68th edition https://www.bp.com/content/dam/bp/business-sites/en/global/corporate/pdfs/energy-economics/statistical-review/bp-stats-review-2019-full-report.pdf

(3) U.S. Energy Information Administration - EIA - Independent Statistics and Analysis "EIA projects nearly 50% increase in world energy usage by 2050, led by growth in Asia" (2020). https://www.eia.gov/todayinenergy/detail.php?id=41433#

(4) Statista "Primary Energy Consumption Worldwide By Fuel - 2018" T. Wang - https://www.statista.com/statistics/265619/primary-energy-consumption-worldwide-by-fuel/

(5) IRENA (2019), *Global energy transformation: A roadmap to 2050 (2019 edition)*, International Renewable Energy Agency, Abu Dhabi.

(6) McKinsey Global Institute, Global Energy Perspective 2019 : Reference Case. Energy Insights, 31 (2019).

(7) B. Novakovic, A. Nasiri, in Electric Renewable Energy Systems (Elsevier Inc., 2016), pp. 1–20.

(8) D. Bruce, K. Haresh, T. Jean-Marie, Electrical Energy Storage for the Grid: A Battery of Choices. Science. 334, 928–935 (2011).

(9) G. L. Soloveichik, Battery Technologies for Large-Scale Stationary Energy Storage. *Annual Review of Chemical and Biomolecular Engineering*. 2, 503–527 (2011).

(10) Schmidt, O., Hawkes, A., Gambhir, A. *et al*. The future cost of electrical energy storage based on experience rates. *Nat Energy* **2**, 17110 (2017).

(11) B. Dunn, H. Kamath, J. M. Tarascon, Electrical energy storage for the grid: A battery of choices. Science. 334 (2011), pp. 928–935.

(12) Chang, L., & Hang Hu, Y. (2018). 2.21 Supercapacitors. Comprehensive Energy Systems, 663–695.

(13) M. S. Halper, J. C. Ellenbogen, Supercapacitors: A Brief Review. MITRE Nanosystems Group, 1–34 (2006).

(14) Z. Yang et al., Electrochemical energy storage for green grid. Chemical Reviews. 111 (2011), pp. 3577–3613.

(15) M. Winter, R. J. Brodd, What are batteries, fuel cells, and supercapacitors? Chemical Reviews. 104, 4245–4269 (2004).

(16) S. M. J. Zaidi, M. A. Rauf, in Polymer Membranes for Fuel Cells (Springer US, 2009), pp. 1–6.

(17) Yan, Q., H. Toghiani, H. Causey, "Steady state and dynamic performance of proton exchange membrane fuel cells (PEMFCs) under various operating conditions and load changes", J. Power Sources 161 (2006) 492 – 502.

(18) Smitha, B., S. Sridhar, A. A. Khan, "Solid polymer electrolyte membranes for fuel cell applications — A review", J. Membr. Sci. 259 (2005) 10 – 26.

(19) Kordesch, K. V., G. R. Simader, "Environmental impact of fuel cell technology", Chem. Rev. 95 (1995) 191 – 207.

(20) N. Gallandat, K. Romanowicz, A. Züttel, An Analytical Model for the Electrolyser Performance Derived from Materials Parameters. Journal of Power and Energy Engineering. 05, 34–49 (2017).

(21) Manzoor Bhat, Z., Thimmappa, R., Devendrachari, M.C., Kottaichamy, A.R., Shafi, S.P., Varhade, S., Gautam, M., and Thotiyl, M.O. (2018). Fuel Exhaling Fuel Cell. Journal of Physical Chemistry Letters 9, 388–392.

(22) Q. Lei, B. Wang, P. Wang, S. Liu, Hydrogen generation with acid/alkaline amphoteric water electrolysis. *Journal of Energy Chemistry*. **38**, 162–169 (2019

(23) J. Jörissen, K. H. Simmrock, The behaviour of ion exchange membranes in electrolysis and electrodialysis of sodium sulphate. Journal of Applied Electrochemistry. 21, 869–876 (1991).

(24) How Much Water Is There on Earth ? www.usgs.gov/special-topic/water-science-school/science/how-much-water-there-earth?qt-science_center_objects=0.

(25) D. Desai et al., Electrochemical Desalination of Seawater and Hypersaline Brines with Coupled Electricity Storage. ACS Energy Letters. 3, 375–379 (2018).

(26) B. Pisarska et al., Application of electro-electrodialysis for processing of sodium sulphate waste solutions containing organic compounds: Preliminary study. Journal of Cleaner Production. 142, 3741–3747 (2017).

(27) Abernathy, C. et al. Drinking Water Advisory : Consumer Acceptability Advice and Health Effects Analysis. EPA 1–34 (2003).

(28) Sulfate in Drinking-Water - World Health Organization. www.who.int/water_sanitation_health/dwq/chemicals/sulfate.pdf.

(29) Shannon, M., Bohn, P., Elimelech, M. et al. Science and technology for water purification in the coming decades. Nature 452, 301–310 (2008).

(30) Service, R. F. Desalination Freshens Up. Science 313, 1088–1090 (2006).

(31) S. J. Kim, S. H. Ko, K. H. Kang, J. Han, Direct seawater desalination by ion concentration polarization. Nature Nanotechnology. 5, 297–301 (2010).

(32) L. F. Greenlee, D. F. Lawler, B. D. Freeman, B. Marrot, P. Moulin, Reverse osmosis desalination: Water sources, technology, and today's challenges. Water Research. 43 (2009), pp. 2317–2348.

(33) Review of the Desalination and Water Purification Technology Roadmap (National Academies Press, 2004).

(34) A. Al-Karaghouli, L. L. Kazmerski, Energy consumption and water production cost of conventional and renewable-energy-powered desalination processes. Renewable and Sustainable Energy Reviews. 24 (2013), pp. 343–356.

(35) M. A. Anderson, A. L. Cudero, J. Palma, Capacitive deionization as an electrochemical means of saving energy and delivering clean water. Comparison to present desalination practices: Will it compete? Electrochimica Acta. 55 (2010), pp. 3845–3856.

(36) N. Tzanetakis, W. Taama, K. Scott, Salt splitting in a three-compartment membrane electrolysis cell. Filtration and Separation. 39, 30–38 (2002).

(37) Y. Oztekin, N. Karadayi, Z. Yazicigil, Salt splitting process application. Desalination and Water Treatment. 22, 187–192 (2010).

(38) Yazicigil, Z. Salt splitting with cation-exchange membranes. Desalination 212, 70–78 (2007).

(39) S. M. Davis, G. E. Gray, P. A. Kohl, Candidate membranes for the electrochemical salt-splitting of Sodium Sulfate. Journal of Applied Electrochemistry. 38, 777–783 (2008).

(40) A. W. Bott, Controlled Current Techniques. *Current Separations*. **18**, 125–127 (2000).

(41) FOR AEM Technical Data Sheet – fumasep FAA-3-50 https://fuelcellstore.com/spec-sheets/fumasep-faa-3-50-technical-specifications.pdf

FOR CEM Technical Data Sheet- Nafion® 211: fuelcellstore.com/nafion-211

(42) Bureau of Reclamation. "Central California Area Office." *Water Facts - Worldwide Water | Bureau of Reclamation*, www.usbr.gov/mp/arwec/water-facts-ww-water-sup.html.

(43) "Sea Water." *ScienceDaily*, ScienceDaily, www.sciencedaily.com/terms/seawater.htm.

(44) O. Lefebvre, R. Moletta, Treatment of organic pollution in industrial saline wastewater: A literature review. *Water Research*. **40** (2006), pp. 3671–3682.

(45) L. P. M. Lamers, H. B. M. Tomassen, J. G. M. Roelofs, Sulfate-induced eutrophication and phytotoxicity in freshwater wetlands. *Environmental Science and Technology*. **32**, 199–205 (1998).

(46) P. Bajpai, P. Bajpai, in *Pulp and Paper Industry* (2015), pp. 25–273.

(47) *EPA*, Environmental Protection Agency, Health Effects from Exposure to High Levels of Sulfate in Drinking Water Study (1999).

(48) W. D. Heizer *et al.*, Intestinal effects of sulfate in drinking water on normal human subjects. *Digestive Diseases and Sciences*. **42**, 1055–1061 (1997).

(49) B. Rahimi, A. Christ, K. Regenauer-Lieb, H. T. Chua, A novel process for low-grade heat-driven desalination. *Desalination*. **351**, 202–212 (2014).

(50) A. M. Bilton, R. Wiesman, A. F. M. Arif, S. M. Zubair, S. Dubowsky, On the feasibility of community-scale photovoltaic-powered reverse osmosis desalination systems for remote locations. *Renewable Energy*. **36**, 3246–3256 (2011).

(51) K. P. Lee, T. C. Arnot, D. Mattia, A review of reverse osmosis membrane materials for desalination-Development to date and future potential. *Journal of Membrane Science*. **370** (2011), pp. 1–22.